Journal of Medicinal Chemistry

Freie Universität Berlin

Article

Radiolabeled dibenzodiazepinone-type antagonists give evidence of dualsteric binding at the M muscarinic acetylcholine receptor

Andrea Pegoli, Xueke She, David Wifling, Harald Hübner, Günther Bernhardt, Peter Gmeiner, and Max Keller

J. Med. Chem., **Just Accepted Manuscript** • DOI: 10.1021/acs.jmedchem.6b01892 • Publication Date (Web): 07 Apr 2017

ACS Publications

Journal of Medicinal Chemistry is published by the American Chemical Society. 1155 Sixteenth Street N.W., Washington, DC 20036

Radiolabeled dibenzodiazepinone-type antagonists give evidence of dualsteric binding at the M_2 muscarinic acetylcholine receptor

Andrea Pegoli,[†] *Xueke She,*[†] *David Wifling,*[†] *Harald Hübner,*[‡] *Günther Bernhardt,*[†] *Peter Gmeiner,*[‡] *and Max Keller*,*[†]

[†]*Institute of Pharmacy, Faculty of Chemistry and Pharmacy, University of Regensburg, Universitätsstr. 31, D-93053 Regensburg, Germany.*

[‡]*Department of Chemistry and Pharmacy, Emil Fischer Center, Friedrich Alexander University, Schuhstr. 19, D-91052 Erlangen, Germany.*

ABSTRACT

The dualsteric ligand approach, aiming at ligands with improved subtype selectivity, has been increasingly applied to muscarinic receptors (MRs). In this article we present the synthesis and characterization of a M_2R subtype-preferring radiolabeled dibenzodiazepinone-type antagonist ([^{3}H]UNSW-MK259, [^{3}H]**19**) and its homodimeric analog [^{3}H]UR-AP060, ([^{3}H]**33**). Saturation binding studies at the M_2R, using the orthosteric antagonist atropine to determine unspecific binding, proved that the monomeric and the dimeric compound bind to the orthosteric binding site (apparent K_d: 0.87 and 0.24 nM, respectively). Various binding studies with [^{3}H]**19** and [^{3}H]**33** at the M_2R, for instance, saturation binding experiments in the presence of the allosteric MR modulators W84 (**8**) or LY2119620 (**9**) (Schild-like analysis) suggested a competitive mechanism between the allosteric modulator and the dibenzodiazepinone derivatives, and thus a dualsteric binding mode of both **19** and **33.** This was consistent with the results of M_2R MD simulations (≥2 μs) performed with **19** and **33**.

Introduction

In humans, the family of muscarinic acetylcholine receptors (M receptors, MRs) comprises five subtypes (M_1R-M_5R), which belong to the GPCR superfamily class A and mediate the action of the neurotransmitter acetylcholine in the CNS as well as in the periphery. For instance, the M_2R is expressed in the myocardium mediating a negative chronotropic and inotropic effect and it acts as a presynaptic autoreceptor in both the brain and the periphery.[1] Accordingly, selective M_2R antagonism in the CNS, resulting in enhanced cholinergic transmission, was suggested as an approach to increase cholinergic function in Alzheimer's disease.[2-5] In general, MRs represent important drug targets, however, there is still a need for subtype selective pharmaceuticals acting at MRs, because the development of selective ligands has been challenging due the high conservation of the acetylcholine (orthosteric) binding site. As MRs exhibit several distinct allosteric binding sites, which are less conserved than the orthosteric site[6, 7] these 7-TM receptors emerged as a prototypic receptor class to study allosterism at GPCRs.[8, 9] Numerous allosteric MR modulators were reported (for instance compounds **7**,[10] **8** (W84)[11] and **9** (LY2119620),[12, 13] Figure 1A), but allosteric ligands with high affinity are lacking.[14] Radiolabeled derivatives of **8** and **9** were shown to be valuable molecular tools to investigate the allosteric interaction at the M_2R.[13, 15] The linkage of an orthosteric MR ligand to an allosteric modulator, called the dualsteric (or bitopic[16]) ligand approach, was suggested as a promising strategy to develop subtype selective MR ligands.[8, 14, 17-21] The rational design of dualsteric MR ligands is supposed to benefit from the recently reported crystal structures of the M_1, M_2, M_3, and M_4 receptor.[7, 22-24] Linking of non-selective MR ligands with allosteric modulators was reported to result in dualsteric M_2R ligands with peculiar pharmacological profiles with respect to subtype binding, the nature of allosteric cooperativity and functional selectivity (for instance **12**-**16**, Figure 1B).[25-29]

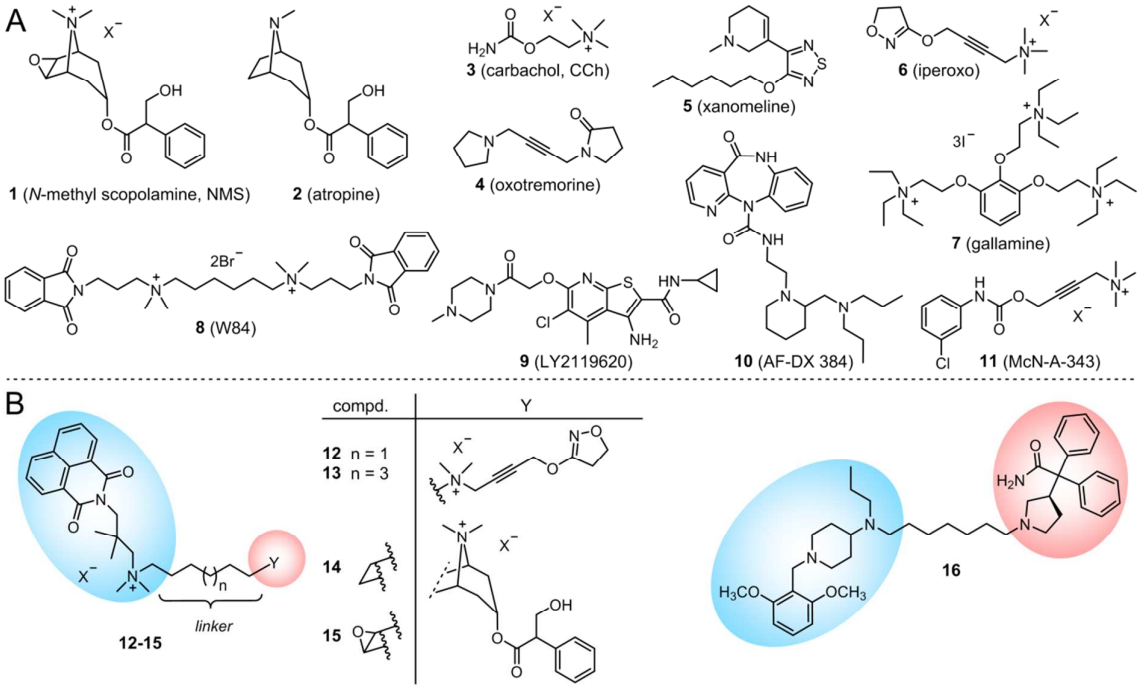

Figure 1. (A) Structures of reported M_2R antagonists (**1**, **2**, **10**), agonists (**3**-**6**, **11**) and allosteric modulators (**7**-**9**). Compounds **10** and **11** were also reported to bind to the allosteric vestibule of the M_2R.[30, 31] (B) Examples of rationally designed dualsteric M_2R ligands obtained by connecting orthosterically (red) with allosterically binding ligands (blue) through a linker.[27, 29]

Recently, a series of dibenzodiazepinone-type M_2R subtype-preferring antagonists, derived from **17** (Figure 2A), including two homodimeric compounds (**20** and **21**, Figure 2A), were reported.[32] Compounds **20** and **21** showed the highest M_2R affinity (for K_i values see Table 1) and their retarding effect on the dissociation of [^{3}H]NMS from the M_2R was more pronounced compared with monomeric derivatives (**18**, **19**, Figure 2A) indicating an involvement of allosteric binding sites in the interaction of these compounds with the M_2R.[32] These findings are supported by previous reports on the M_2R binding profile of **10** (AF-DX 384)[33] (Figure 1A),[30] which is a close structural analog to **17** (Figure 2A) and was suggested to interact with the orthosteric as well as with the allosteric binding site. Notably, the use of the tritiated form of **10** proved to be a valuable approach to investigate the binding mode.[30]

The present study aims at the elucidation of the binding mode of complex ligands such as the dibenzodiazepinone derivatives **20** and **21** at the M_2R. For this purpose we designed

congeners of **20** and **21**, which can be conveniently prepared as tritium-labeled ligands, by introducing a branched ring structure in the center of the molecule intended to bear the radiolabel (Figure 2B). For comparison, the tritium-labeled form of **19**, representing the monomeric counterpart of the dimeric ligand **20** (Figure 2A), was synthesized and also studied in saturation binding assays including experiments in the presence of allosteric modulators (Schild-like analysis). Moreover, kinetic investigations, equilibrium competition binding studies and molecular dynamics simulations were performed.

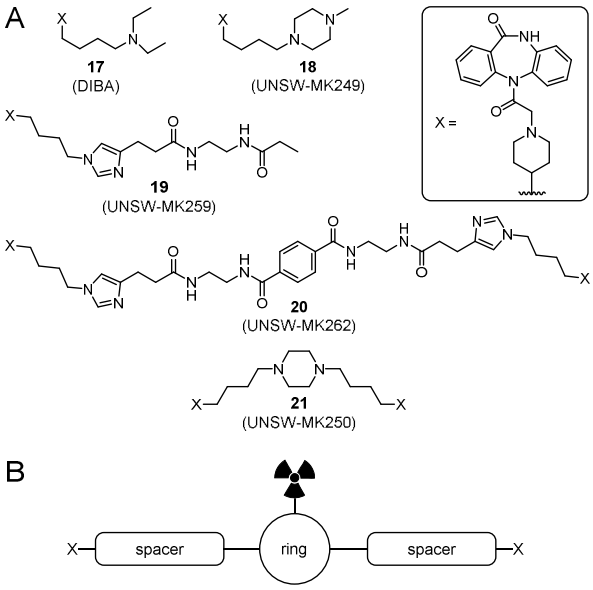

Figure 2 (A) Structures of recently reported DIBA-derived MR antagonists, including the homodimeric compounds **20** and **21**. (B) Schematic presentation of radiolabeled homodimeric DIBA derivatives, used as tools to investigate the binding mode at the M_2R.

Results and Discussion

Chemistry. The preparation of the homodimeric dibenzodiazepinone derivative **33**, containing an isophtalic acid moiety in the center, is outlined in Scheme 1. The crucial building block **29**, namely N-Boc protected aminomethylated isophtalic acid, was synthesized from **22** via azide **27**, following reported procedures with minor modifications (Scheme 1).[34, 35] Amidation of **29** with amine **30**,[32] using HBTU/HOBt as coupling reagent, and subsequent

removal of the Boc group gave amine **31**, which represents a precursor for the preparation of differently functionalized dimeric MR ligands (e.g. radiolabeled and fluorescence labeled compounds). Propionylation of **31**, using succinimidyl propionate (**32**) afforded **33**, which represents the 'cold' form of a tritium-labeled dimeric MR ligand.

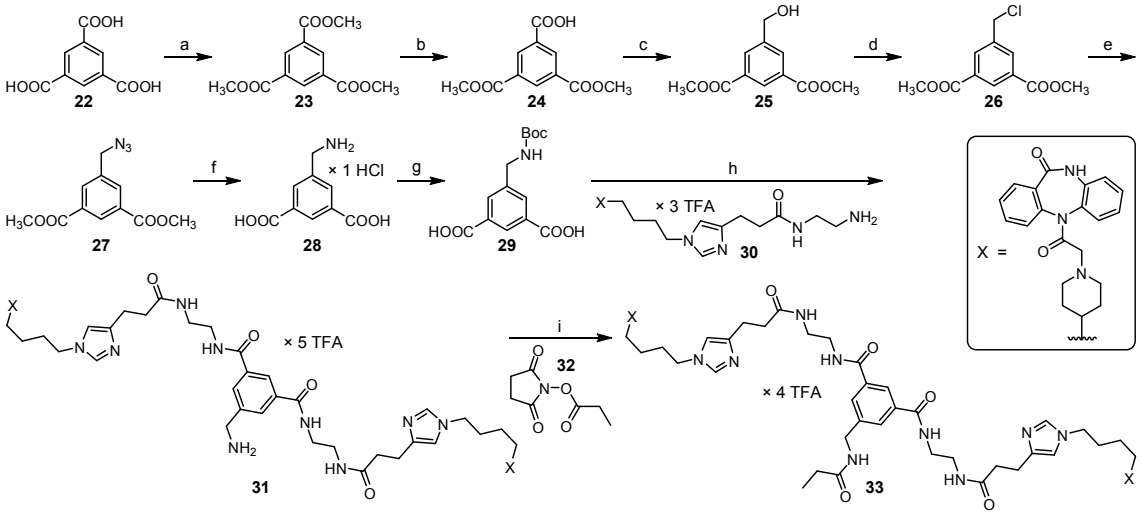

Scheme 1. Synthesis of the homodimeric MR ligand **33**. Reagent and conditions: (a) H_2SO_4, MeOH, reflux, 24 h, 99%; (b) $NaOH_{aq}$ 1 M, MeOH, rt, 18 h, 75%; (c) $(CH_3)_2S{\cdot}BH_3$, THF, rt, 24 h, 87%; (d) $SOCl_2$, reflux, 90 min, 98%; (e) NaN_3, acetone, reflux, 16 h, 96%; (f) (1) triphenylphosphine, H_2O/THF 5:1 (v/v), rt, 10 h, (2) $NaOH_{aq}$ 1 M, rt, 8 h, 71%; (g) di-*tert*-butyldicarbonate, triethylamine, H_2O/dioxane 1:1 (v/v), rt, 12 h, 61%; (h) (1) HOBt, TBTU, DIPEA, DMF, 60°C, 3 h (2) triethylamine/CH_2Cl_2/H_2O 10:10:1 (v/v/v), rt, 3 h, 32%; (i) DIPEA, DMF, rt, 1 h, 90%.

The key intermediates for the synthesis of the homodimeric MR ligand **47**, containing a basic homopiperazine moiety in the center of the molecule, were bromide **38** and homopiperazine derivative **45c** (Scheme 2). Compound **38** was obtained by reduction of the carboxylated piperazine derivative **34** to the corresponding alcohol **35**, followed by *N*-alkylation of **35** with chloride **36** yielding alcohol **37**. The latter was converted to bromide **38** using perbromomethane and triphenylphosphine (Scheme 2). The synthesis of homopiperazine **45c** started with a nitro-Mannich reaction of dibenzylated ethylenediamine (**39**) and nitroethanol (**40**) yielding derivative **41**, which was converted into homopiperazine **42** by a retro-Henry reaction. Reduction of the nitro group in **42** using Raney-Nickel and hydrogen led to primary

amine **43**, which was Boc-protected to obtain intermediate **44** (Scheme 2). Several attempts to debenzylate **44** by hydrogenolysis using 10% Pd/C and methanol or ethanol as solvent, failed due to solvent oxidation to formaldehyde and acetaldehyde, respectively, and formation of the cyclic aminal **45a** and the *N*-alkylated derivative **45b** (identified by NMR spectroscopy and mass spectrometry, data not shown). The use of 2,2,2-trifluoroethanol as solvent, preventing the Pd-catalyzed oxidation of the alcoholic solvent to the corresponding aldehyde,[36] enabled a successful debenzylation of **44**, affording homopiperazine **45c** without by-products. The alkylation of **45c** using bromide **38**, followed by Boc-deprotection, led to the amino-functionalized dimeric dibenzodiazepinone derivative **46**, which was propionylated to give compound **47**, representing the 'cold' form of a tritium-labeled dimeric ligand as well. Imidazolyl propionic acid derivative **50**, representing the terminal moiety of the side chain in **19** (*cf.* Figure 2), was prepared from urocanic acid derivative **48** (Scheme 2),[32] which was converted to **49** by hydrogenolytic reduction of the 'acrolein' double bond under acidic conditions resulting in a simultaneous cleavage of the Boc group (Scheme 2). Propanoylation of **49** using **32** yielded compound **50**. The homodimeric dibenzodiazepinone derivative **52** was prepared by alkylation of piperazine with chloride **36** (Scheme 2).

The chemical stability of compounds **19**, **33** and **47** was investigated in PBS (pH 7.4) at 23 °C over a period of 48 h. These dibenzodiazepinone derivatives showed excellent stabilities (see supporting information, Figure S1).

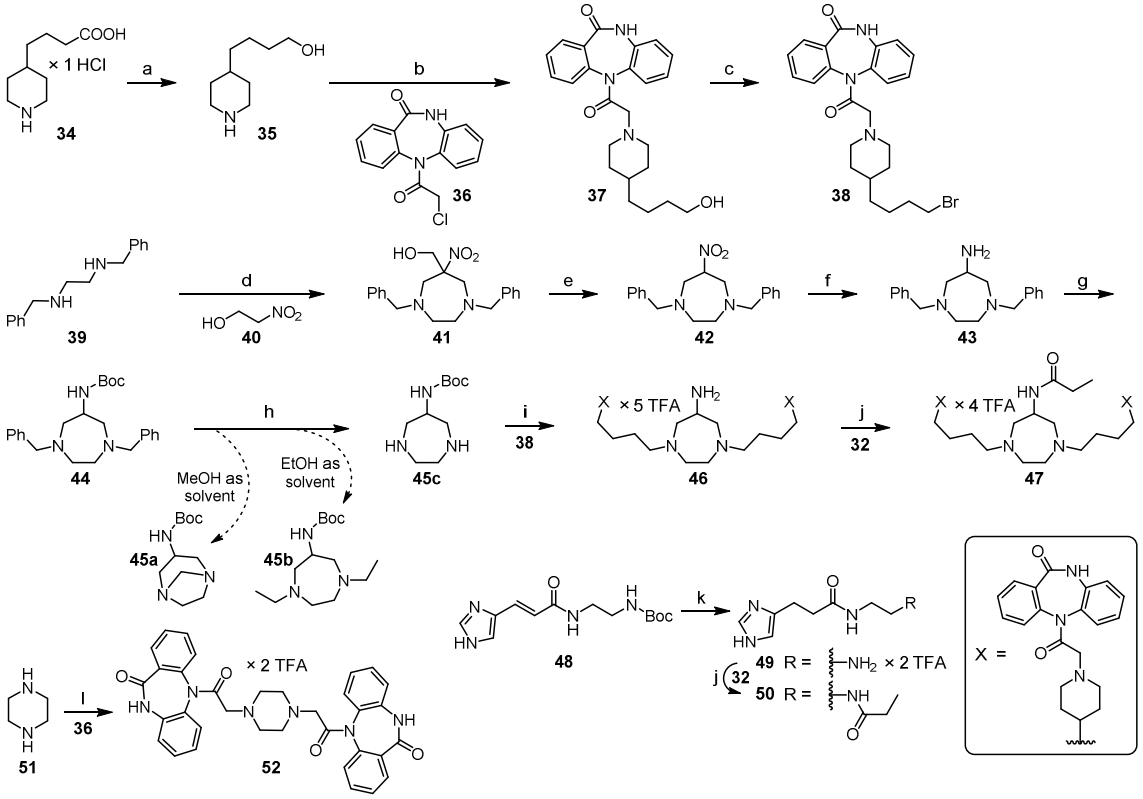

Scheme 2. Synthesis of the homodimeric MR ligands **47** and **52** and the imidazolyl propionic acid derivative **50**. Reagent and conditions: (a) $LiAlH_4$, THF, 0°C/reflux, 12h, 89%; (b) K_2CO_3, acetonitrile, reflux, 5 h, 43%; (c) CBr_4, triphenylphosphine, CH_2Cl_2, -5°C/5°C, 5 h, 79%; (d) paraformaldehyde, EtOH/toluene 1:1 (v/v), reflux, 6 h, 87%; (e) potassium *tert*-butanolate, anhydrous THF, rt, 30 min, 95%; (f) H_2, Raney-Nickel, EtOH, rt, 12 h, 44%; (g) di-*tert*-butyldicarbonate, CH_3Cl, 0°C/rt, 5 h, 81%; (h) Pd/C (10%), H_2, 2,2,2-trifluoroethanol, 1 atm, rt, 12 h, 85%; (i) (1) K_2CO_3, DMF, 120 °C (microwave), 1.5 h (2) CH_2Cl_2/TFA/H_2O 10:10:1 (v/v/v), rt, 3 h, 37%; (j) DIPEA, DMF, rt, 1-1.5 h, 72% (**47**), 43% (**50**); (k) Pd/C (10%), H_2, MeOH/TFA 1:1 (v/v), 7.9 atm, rt, 12 h, 90%; (l) K_2CO_3, acetonitrile, 130°C (microwave), 30 min, 21%.

Synthesis of radiolabeled dibenzodiazepinone derivatives. The tritium-labeled dibenzodiazepinone derivatives [^{3}H]**19**, [^{3}H]**33** and [^{3}H]**47** were obtained by treatment of an excess of the amine precursors **30**, **31** and **46**, respectively, with commercially available succinimidyl [^{3}H]propionate ([^{3}H]**32**) in the presence of DIPEA (Figure 3A). In order to facilitate the purification of [^{3}H]**47**, the excess of amine precursor **46** was 'quenched' by the addition of succinimidyl 4-fluorobenzoate (**53**), resulting in the formation of **54**, which could be conveniently separated from [^{3}H]**47** (Fig. 3B). Purification by RP-HPLC afforded all radioligands in high radiochemical purity (99%, Figure 3C-E). [^{3}H]**19**, [^{3}H]**33** and [^{3}H]**47**

proved to be stable upon storage in EtOH/H_2O 1:1 (v/v) at −20 °C (Figure S2, Supporting Information).

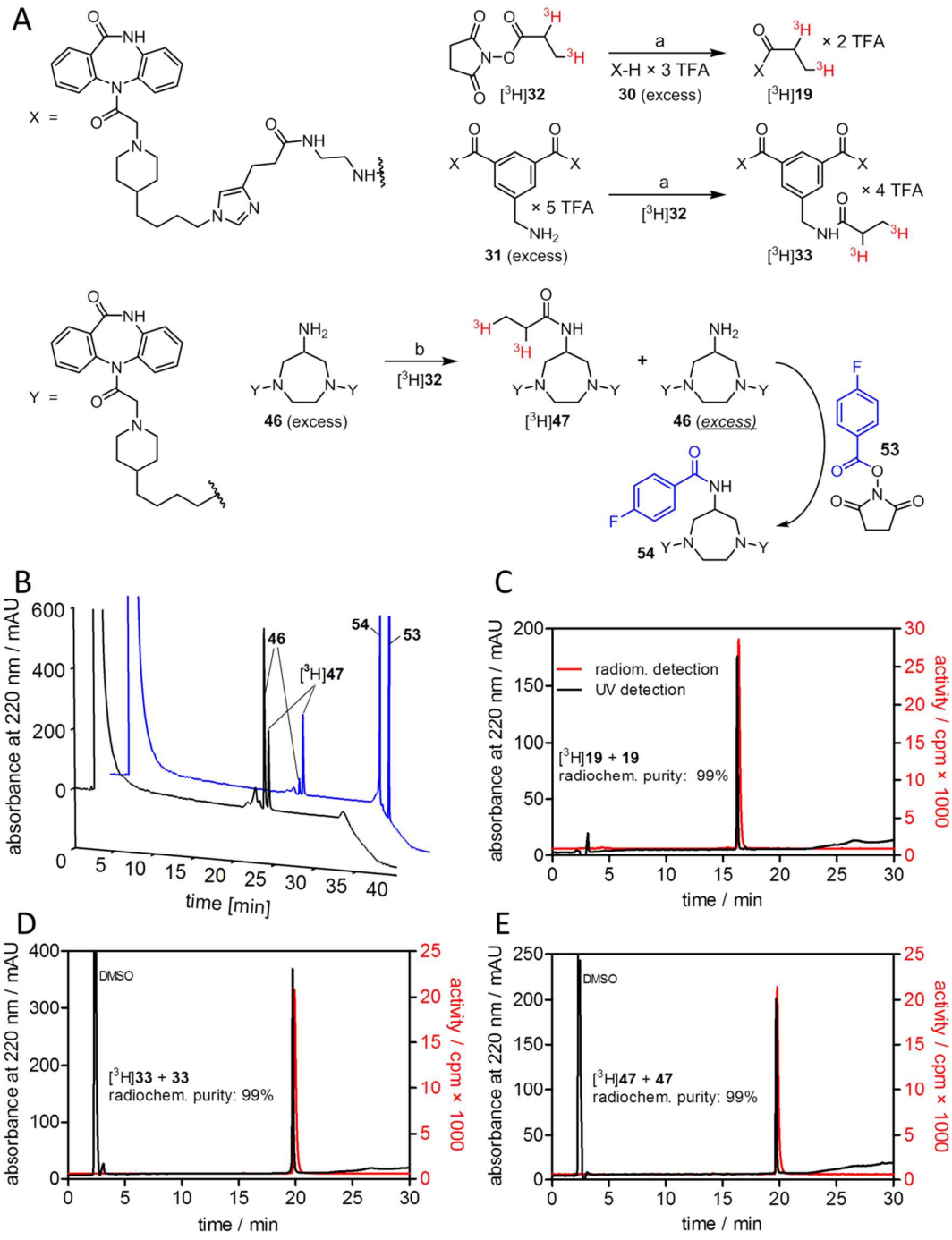

Figure 3. (A) Synthesis of the MR radioligands [^{3}H]**19**, [^{3}H]**33** and [^{3}H]**47** by [^{3}H]propionylation of the amine precursor **30**, **31** and **46**, respectively, using succinimidyl [^{3}H]propionate ([^{3}H]**32**). Reagents and conditions: (a) DIPEA, DMF, rt, 60 min, 39% ([^{3}H]**19**), 32% ([^{3}H]**33**); (b) (1) DIPEA, DMF, rt, 45 min, (2) **53**, rt, 60 min, 38%. The excess of **46** was 'quenched' by 4-fluorobenzoylation to facilitate the purification of [^{3}H]**47** (*cf.* B).

(B) RP-HPLC monitoring of the synthesis of [^{3}H]**47** before (black line) and after (blue line) addition of the active ester **53**. (C-D) RP-HPLC analysis (conditions see experimental section) of [^{3}H]**19** (0.23 μM) (C), [^{3}H]**33** (0.20 μM) (D) and [^{3}H]**47** (0.20 μM) (E), each spiked with the 'cold' analog (**19** and **33**: 5 μM; **47**: 3 μM) analyzed 2 days after synthesis.

Equilibrium competition binding studies with [^{3}H]NMS. M_1-M_5 receptor affinities of the dimeric dibenzodiazepinone derivatives **33** and **47** were investigated in equilibrium competition binding experiments using [^{3}H]NMS (structure of the 'cold' analog see Figure 1A) as orthosterically binding radioligand. The MR binding constants (pK_i values) are presented in Table 1 in comparison with previously reported M_1R-M_5R affinities of **18-21**. The transformation of the structures of **20** and **21** to **33** and **47**, respectively, by the introduction of a branched central linker moiety (Figure 2, Schemes 1 and 2) resulted only in a marginally decrease in M_2R affinity (Figure S3, Supporting Information), and in a MR subtype selectivity profile comparable to that of the parent compounds **20** and **21** (Table 1). Steep curve slopes were observed for **33** at the M_1R (slope = −1.8) and M_2R (slope = −2.2) indicating a complex mechanism of binding (e.g. the involvement of more than one binding site). Moreover, equilibrium binding of [^{3}H]NMS at the M_2R in the presence of homodimeric dibenzodiazepinone derivative **52** (*cf.* Scheme 2) and the reported M_2R allosteric modulator **9** was investigated. Compared to the homodimeric ligands **33** and **47**, in which the pharmacophores are separated by complex linker moieties, the decrease in [^{3}H]NMS binding caused by compound **52** was considerably less pronounced by more than four orders of magnitude (Supporting Information, Figure S4A). Similarly, the allosteric modulator **9**, reported to exhibit a negative cooperativity with NMS,[23] showed a weak inhibitory effect on [^{3}H]NMS equilibrium binding (Supporting Information, Figure S4B).

Table 1. M_1-M_5 receptor affinities (pK_i values) of the DIBA derivatives **18-21**, **33** and **47**, obtained from equilibrium competition binding studies with [^{3}H]NMS at live CHO-hM_xR cells (x = 1-5).

compd.	M_1R		M_2R		M_3R		M_4R		M_5R	
	pK_i	slope[a]	pK_i	slope[a]	pK_i	slope[a]	pK_i	slope[a]	pK_i	slope[a]
18	8.01 ± 0.08	1.13 ± 0.10	9.17 ± 0.06	-1.25 ± 0.08	7.11 ± 0.08	-0.92 ± 0.09	8.49 ± 0.11	-0.99 ± 0.09	6.36 ± 0.09	-0.97 ± 0.14
19	8.07 ± 0.06	-1.11 ± 0.11	9.12 ± 0.05	-1.19 ± 0.06	7.22 ± 0.08	-1.09 ± 0.08	8.63 ± 0.02	-0.86 ± 0.03	6.75 ± 0.08	-0.68 ± 0.11
20	8.91 ± 0.05	-1.56 ± 0.08[b]	9.71 ± 0.05	-1.27 ± 0.12	7.88 ± 0.03	-1.30 ± 0.09[b]	9.19 ± 0.08	-1.17 ± 0.14	7.44 ± 0.10	-1.46 ± 0.18
21	9.00 ± 0.04	-1.32 ± 0.09[b]	9.51 ± 0.19	-2.01 ± 0.07[b]	8.17 ± 0.03	-1.05 ± 0.14	8.97 ± 0.08	-1.32 ± 0.17	7.64 ± 0.08	-1.09 ± 0.09
33	8.82 ± 0.10	-1.81 ± 0.16[b]	9.39 ± 0.05	-2.17 ± 0.19[b]	7.81 ± 0.01	-1.19 ± 0.11	9.33 ± 0.11	-1.17 ± 0.06	7.64 ± 0.04	-0.95 ± 0.13
47	8.15 ± 0.06	-1.29 ± 0.12	9.15 ± 0.01	-1.40 ± 0.06[b]	6.70 ± 0.06	-1.15 ± 0.06	8.44 ± 0.09	-0.87 ± 0.08	7.11 ± 0.18	-1.06 ± 0.13

Presented are mean values ± SEM from 3-9 independent experiments (each performed in triplicate). K_d values[32] / applied concentrations of [^{3}H]NMS: M_1: 0.12 / 0.2 nM; M_2: 0.090 / 0.2 nM; M_3: 0.089 / 0.2 nM; M_4: 0.040 / 0.1 nM; M_5: 0.24 / 0.3 nM. Data of **18-21** were previously reported as pIC_{50} values by Keller *et al*.[32] and were re-analyzed to obtain pK_i values. [a]Curve slope of the four-parameter logistic fit. [b]Slope different from unity ($P < 0.05$).

Functional studies. The monomeric dibenzodiazepinone derivative **19** and the homodimeric congener **33** were investigated in an IP1 accumulation assay using HEK-293 cells transiently transfected with the human M_2R and the hybrid G-protein $G\alpha_{qi5\text{-}HA}$. **19** and **33** did not elicit IP1 accumulation when studied in agonist mode (Figure 4A), that is, they were incapable of stabilizing a G-protein activating conformation of the M_2R. In antagonist mode, **19** and **33** completely inhibited IP1 accumulation elicited by **3** (0.3 μM, ≈ EC_{80}), proving these compounds to be M_2R antagonists as previously reported for **10** (Figure 4B).[30] It is a matter of speculation why the pK_b values of **19** and **33** (Figure 4B) were lower than the pK_i values presented in Table 1. Presumably, this can be attributed to the different experimental conditions (different temperature (37 *vs*. 23 °C), incubation time (1 h *vs*. 3 h) and readout (radioligand binding *vs*. functional response)). In addition, the inhibiting effects of **19** and **33** on the IP1 accumulation elicited by **3**, used at various fixed concentrations (0.1, 1 and 10 μM), were determined (Figure 4C and 4D). The inhibition curves reached throughout 0% IP1

accumulation, indicating a competitive mechanism between the orthosteric agonist **3** and the dibenzodiazepinone derivatives **19** and **33**.

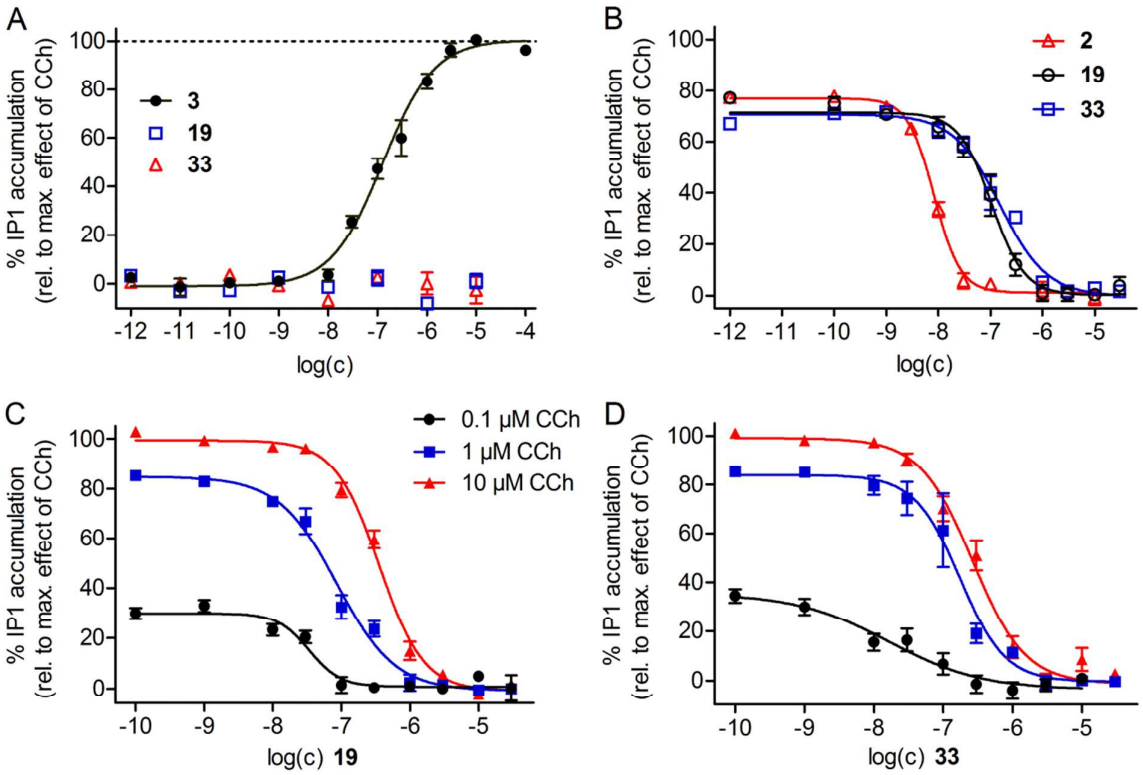

Figure 4. Investigation of M_2R agonism and antagonism of compounds **19** and **33** in an IP1 accumulation assay using HEK-hM_2-G$\alpha_{qi5\text{-}HA}$ cells. (A) Concentration-dependent effect of **3**, **19** and **33** on the accumulation of IP1. **19** and **33** elicited no response. pEC_{50} of **3**: 6.93 ± 0.09 (mean ± SEM from 8 independent experiments performed in duplicate). (B) Concentration-dependent inhibition of the IP1 accumulation (induced by **3**, 0.3 µM) by **2**, **19** and **33**. Corresponding pK_b values: **2**: 8.63, **19**: 7.53, **33**: 7.36. (C) Concentration-dependent inhibition of the IP1 accumulation (induced by **3**, 0.1, 1 and 10 µM) by **19**. Corresponding pIC_{50} values: 7.47, 7.07 and 6.45, respectively. Concentration-dependent inhibition of the IP1 accumulation (induced by **3**, 0.1, 1 and 10 µM) by **33**. Corresponding pIC_{50} values: 7.78, 6.76 and 6.58, respectively. Data in B-C represent the means ± SEM from at least four independent experiments (each performed in duplicate).

Characterization of [^{3}H]19, [^{3}H]33 and [^{3}H]47. Saturation binding experiments with the radiolabeled dibenzodiazepinone derivatives [^{3}H]**19**, [^{3}H]**33** and [^{3}H]**47** were performed at intact adherent CHO-hM_2 cells in white-transparent 96-wells plates revealing apparent K_d values of 0.87, 0.91 and 8.4 nM, respectively (mean values from at least three independent

experiments performed in triplicate) (Figure 5A, 5B and 5E). Whereas unspecific binding was very low in case of the monomeric ligand [^{3}H]**19** (<5% at the K_d), drastically increased unspecific binding (>60%) was a characteristic of the dimeric ligands [^{3}H]**33** and [^{3}H]**47** (Figure 5B and 5E). Saturation binding studies with [^{3}H]**33** and [^{3}H]**47** performed with intact CHO-hM_2 cells in suspension ([^{3}H]**33**, Figure 5C) or with CHO-hM_2 cell homogenates ([^{3}H]**33** and [^{3}H]**47**, Figure 5D and 5F, respectively), precluding unspecific binding of the radioligand to the microplate, resulted in considerably lower unspecific binding (<15% at K_d), indicating that the dimeric ligands **33** and **47** strongly adsorb to polystyrene tissue-culture treated microplates (for experimental protocols see experimental section). The apparent K_d values amounted to 0.31 nM ([^{3}H]**33**, suspended cells), 0.24 nM ([^{3}H]**33**, homogenates) and 4.6 nM ([^{3}H]**47**, homogenates) (mean values from at least three independent experiments performed in triplicate). Worth mentioning, saturation binding studies performed with [^{3}H]NMS, [^{3}H]**19** and [^{3}H]**33** on the same day, yielded comparable maximum numbers of M_2R binding sites per well (B_{max} values) independent of using cell homogenates or intact cells (Supporting Information, Figure S5). These results suggested a ligand-receptor stoichiometry of 1:1 for [^{3}H]NMS, the monomeric ligand [^{3}H]**19** and the dimeric ligand [^{3}H]**33**. In addition, saturation binding experiments were performed with [^{3}H]**33** at live CHO-hM_4 cells resulting in a K_d value of 0.67 nM (mean value from four independent experiments performed in triplicate) (*cf*. Supporting Information, Figure S6).

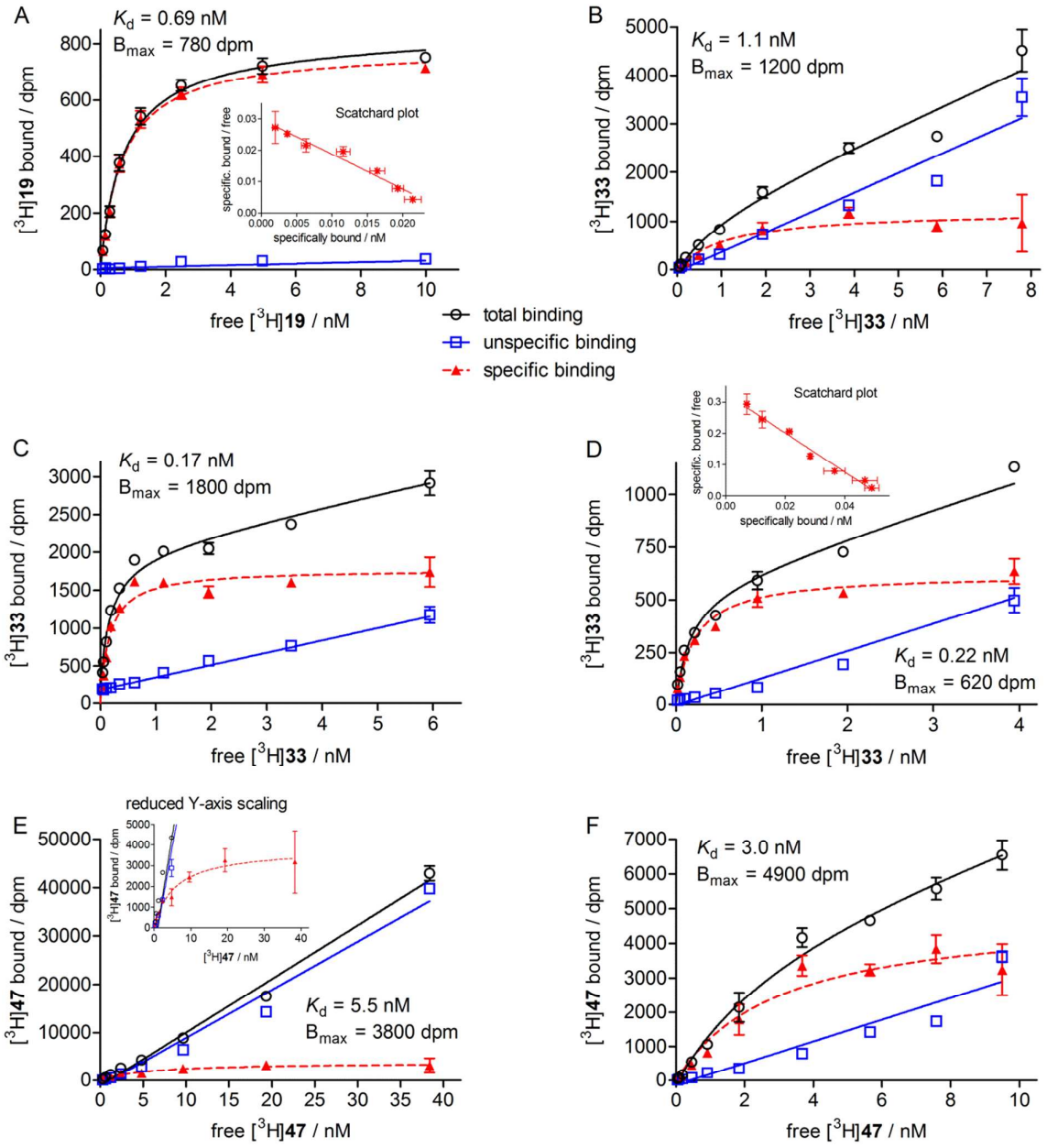

Figure 5. Representative saturation isotherms (in red) of specific M_2R binding of [^{3}H]**19** (A), [^{3}H]**33** (B-D) and [^{3}H]**47** (E, F) obtained from experiments either performed with live adherent CHO-hM_2 cells (A, B, E), live CHO-hM_2 cells in suspension (C) or CHO-hM_2 cell homogenates (D, F). Unspecific binding was determined in the presence of the orthosterically binding MR antagonist atropine (500-fold excess). Scatchard transformations are depicted for the optimized binding assay conditions (A, D). Experiments were performed in triplicate. Specific binding data were analyzed by an equation describing a one-site binding. Error bars of specific binding and error bars in the Scatchard plots represent propagated errors calculated according to the Gaussian law of errors. Error bars of total and nonspecific binding represent the SEM.

As the orthosteric antagonist **2**, used to determine unspecific binding, was able to completely prevent one-site (monophasic) specific binding of [^{3}H]**19**, [^{3}H]**33** and [^{3}H]**47** to the M_2R, these data strongly suggest that the dibenzodiazepinone derivatives **19**, **33** and **47** address the orthosteric binding site of the M_2R. A putative involvement of a second binding site in M_2R binding of the dimeric radioligand [^{3}H]**33**, indicated by the steep slope factor presented in Table 1, was not obvious from saturation binding experiments with [^{3}H]**33**, which yielded monophasic saturation isotherms and a linear Scatchard plot (Figure 5C and 5D).

Due to its inappropriate physicochemical properties (high unspecific binding) and the discrepancy between the K_d ([^{3}H]**47**) and the K_i (**47**) values (*cf.* Table 3), [^{3}H]**47** was not considered with respect to further characterization, contrary to the monomeric radioligand [^{3}H]**19** and its dimerized analog [^{3}H]**33**. The association of both, [^{3}H]**19** and [^{3}H]**33**, to the M_2R (live cells) could be described by a monophasic fit resulting in comparable k_{on} rates (Figure 6A, 6C, Table 2). By contrast, the dissociation from the M_2R (live cells) was different: whereas the monomeric ligand [^{3}H]**19** completely dissociated with a half-life of 71 min (monophasic decline), the dissociation of the dimeric dibenzodiazepinone derivative [^{3}H]**33** was incomplete, reaching a plateau at 67% of initially bound radioligand. Dissociation experiments with [^{3}H]**33** at CHO-hM_2 cell homogenates gave comparable results (plateau at 63%; *cf.* Supporting Information, Figure S7). These data suggested in part a (pseudo)irreversible (long lasting) binding of [^{3}H]**33**, which might be attributed to conformational adjustments of the receptor upon ligand binding,[37] or to an enhanced rebinding capability of the dimeric ligand by a simultaneous interaction with two or more binding sites.[38] However, the equilibrium dissociation constant of [^{3}H]**33**, calculated from k_{off} and k_{on} (K_d(kin) = k_{off}/k_{on} = 0.20 nM, Table 2) was in good agreement with the K_d value derived from saturation binding experiments (K_d = 0.31 nM) indicating that [^{3}H]**33** follows in part the law of mass action. Notably, the dissociations of [^{3}H]**19** and [^{3}H]**33** from the M_2R were not or only marginally effected by the allosteric modulator **8** applied at a

'supramaximal' concentration of 100 μM (Figure 6B and 6D), which is consistent with a competitive mechanism between [^{3}H]**19** and **8** as well as [^{3}H]**33** and **8**; in other words, these results preclude a high negative cooperativity between the studied ligands.[39] An overview of the M_2R binding characteristics of [^{3}H]**19** and [^{3}H]**33** is provided in Table 2.

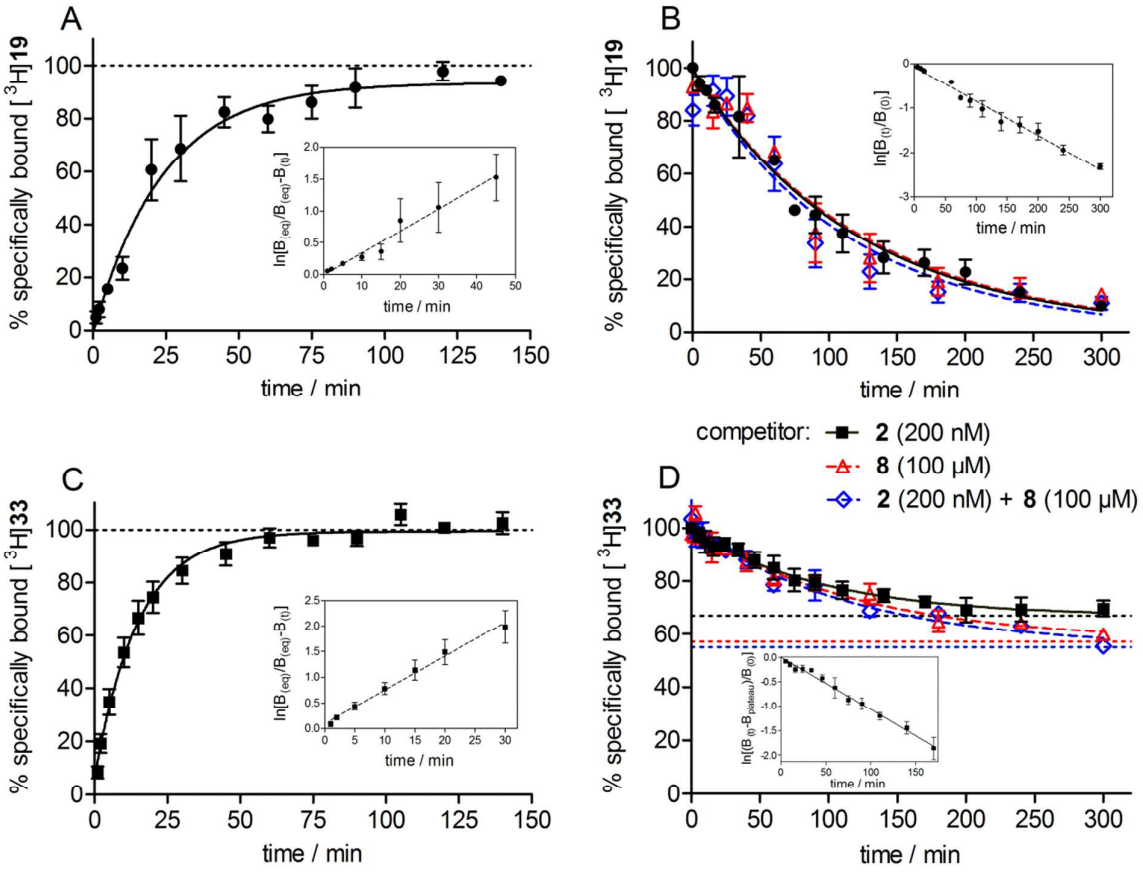

Figure 6. Association and dissociation kinetics of [^{3}H]**19** (A, B) and [^{3}H]**33** (C, D) determined at intact CHO-hM_2 cells at 23 °C. (A) Radioligand (c = 2 nM) association to the M_2R as a function of time (non-linear regression: k_{obs} = 0.042 min^{-1}); inset: ln[$B_{(eq)}$/($B_{(eq)}$−$B_{(t)}$)] versus time, k_{obs} = slope = 0.035 min^{-1}. (B) Radioligand (preincubation: 2 nM, 105 min) dissociation from the M_2R as a function of time, showing complete monophasic exponential decline (non-linear regression: k_{off} = 0.0091 min^{-1}, $t_{1/2}$ = 71 min); inset: ln[$B_{(t)}$/$B_{(0)}$] versus time, slope·(−1) = k_{off} = 0.0077 min^{-1}, $t_{1/2}$ = 90 min. (C) Radioligand (c = 1 nM) association to the M_2R as a function of time (non-linear regression: k_{obs} = 0.067 min^{-1}); inset: ln[$B_{(eq)}$/($B_{(eq)}$-$B_{(t)}$)] versus time, k_{obs} = slope = 0.066 min^{-1}. (D) Radioligand (preincubation: 1 nM, 90 min) dissociation from the M_2R as a function of time, showing incomplete monophasic exponential decline (non-linear regression: k_{off} = 0.011 min^{-1}, $t_{1/2}$ = 66 min, plateau = 67%); inset: ln[($B_{(t)}$-$B_{plateau}$)/$B_{(0)}$] versus time, slope·(−1) = k_{off} = 0.011 min^{-1}, $t_{1/2}$ = 64 min. The dissociation kinetics of [^{3}H]**19** and [^{3}H]**33** were not or only marginally effected by the allosteric modulator **8** at a 'supramaximal' concentration of 100 μM (B, D (open triangles and open diamonds)), indicating a competitive interaction between the radioligands and **8**. Data represent means ± SEM from two or three (B, C, D) or four (A) independent experiments (each performed in triplicate).

Table 2. M_2R binding data of [^{3}H]**19**, [^{3}H]**33** and [^{3}H]**47** (at 23 ± 1 °C).

radioligand	K_i ('cold' analog) [nM][a]	K_d(sat) [nM][b]	K_d(kin) [nM][c]	k_{on} [$min^{-1} \cdot nM^{-1}$][d]	k_{off} [min^{-1}][e] $t_{1/2}$ [min][e]
[^{3}H]**19**	0.76 ± 0.05	0.87 ± 0.01	0.70 ± 0.10	0.013 ± 0.003	0.0091 ± 0.0016 71 ± 7
[^{3}H]**33**	0.41 ± 0.05	0.31 ± 0.08	0.20 ± 0.04	0.056 ± 0.010	0.011 ± 0.001 66 ± 9
[^{3}H]**47**	0.71 ± 0.01	4.6 ± 1.3	n.d	n.d	n.d

[a]Dissociation constant determined by equilibrium competition binding with [^{3}H]NMS at intact CHO-hM_2 cells; mean ± SEM from at least three independent experiments (performed in triplicate). [b]Equilibrium dissociation constant determined by saturation binding at intact CHO-hM_2 cells ([^{3}H]**19** and [^{3}H]**33**) and at CHO-hM_2 cell homogenates ([^{3}H]**47**); mean ± SEM from at least three independent experiments (performed in triplicate). [c]Kinetically derived dissociation constant ± propagated error (K_d(kin) = k_{off}/k_{on}). [d]Association rate constant ± propagated error, calculated from k_{obs}, k_{off} and the applied radioligand concentration (*cf.* Figure 6 and experimental section). [e]Dissociation rate constant and derived half-life (non-linear fit); mean ± SEM from three independent experiments (performed in triplicate).

Binding of the monomeric dibenzodiazepinone derivative **19** to the orthosteric site was further supported by investigating the saturation binding of the orthosteric radioligand [^{3}H]NMS in the presence of **19** (Schild-like analysis). This experiment revealed a parallel rightward shift of the saturation isotherms of [^{3}H]NMS and a slope not different from unity of the corresponding 'Schild' regression, being indicative of a competitive interaction between **19** and the orthosteric radioligand [^{3}H]NMS (Supporting Information, Figure S8).

M_2R equilibrium competition binding with [^{3}H]19 and [^{3}H]33. Selected standard MR agonists (**4**, **5**) antagonists (**1**, **2**, **10**) and allosteric modulators (**7**, **8**) as well as the 'cold' forms of the radioligands (**19**, **33**) were investigated by equilibrium competition binding with [^{3}H]**19** or [^{3}H]**33**. The concentration-dependent effects of the investigated compounds on equilibrium binding of [^{3}H]**19** and [^{3}H]**33**, analyzed by four-parameter logistic fits, are depicted in Figure 7. The lower curve plateaus were throughout not different from 0 ($P > 0.2$), which either suggests a competitive mechanism or a strongly negative cooperativity between the studied compounds and the radiolabeled dibenzodiazepinone derivatives.[40]

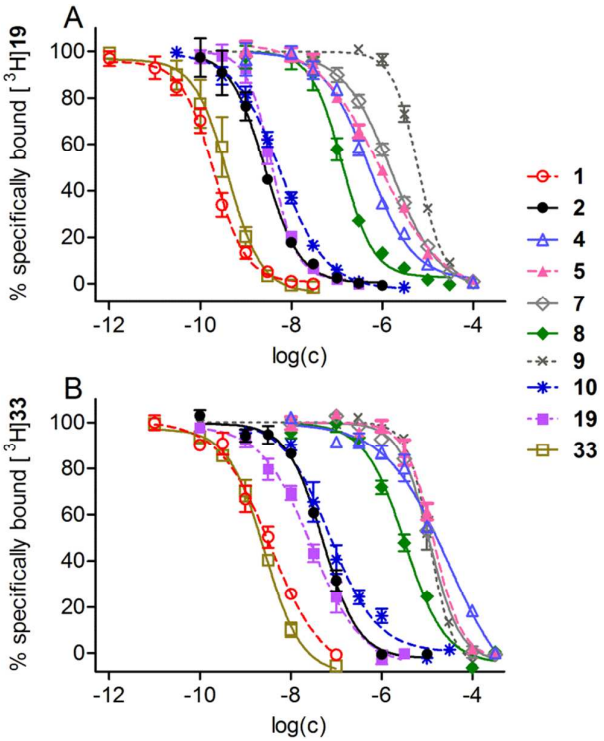

Figure 7. Concentration-dependent effects of various reported orthosteric (**1-5**), allosteric (**7-9**) and dualsteric (**10**, **19**, **33**) MR ligands on M_2R equilibrium binding of [^{3}H]**19** (c = 2 nM, K_d = 0.87 nM) (A) and [^{3}H]**33** (c = 0.5 nM, K_d = 0.24 nM) (B) determined at live CHO-hM_2 cells and at CHO-hM_2 cell homogenates, respectively. Data were analyzed by four-parameter logistic fits. Mean values ± SEM from at least three independent experiments (performed in triplicate).

Generally, pK_i values derived from equilibrium competition binding with [^{3}H]**19** were in good agreement with reported data (Table 3). However, pK_i values determined with the dimeric radioligand [^{3}H]**33** were consistently lower compared to M_2R affinities obtained by the use of [^{3}H]**19**. This can be explained by the (pseudo)irreversible binding of [^{3}H]**33** at the M_2R (*cf.* Figure 6D): in putative equilibrium competition binding experiments a dynamic equilibrium between the receptor and the competing ligands cannot be reached. The fraction of receptor, irreversibly bound to [^{3}H]**33**, is inaccessible for the studied non-labeled ligand. As a consequence, "displacement" of the irreversibly binding radioligand by the non-labeled reversibly binding ligand requires a higher receptor occupancy by the latter (relative to the radioligand) compared to the situation of two reversibly binding competing ligands. Moreover, due to the (pseudo)irreversible binding of [^{3}H]**33**, the apparent K_d value of [^{3}H]**33**,

obtained from saturation binding studies (*cf.* Figure 5D), is presumably lower than the real K_d value, resulting in an underestimation of the affinity of the studied ligand (calculated via Cheng-Prusoff). Additional equilibrium competition binding experiments performed with **4** and **10**, applying a preincubation period of 90 min with the M_2R prior to the addition of [^{3}H]**33**, did not result in an increase in the apparent pK_i of **4** and **10** (data not shown), which is anticipated according to the aforementioned hypothesis.

Table 3. M_2R binding data (pK_i or pIC_{50}) of various orthosteric (**1-5**), allosteric (**7-9**) and dualsteric (**10**, **19**, **33**) MR ligands determined with [^{3}H]**19**, [^{3}H]**33** or [^{3}H]NMS.

Ligand	[^{3}H]**19** pK_i[a]	[^{3}H]**33** pK_i[b]	[^{3}H]NMS pK_i[*] or pIC_{50}[**] (± SEM)
1	10.2 ± 0.10	8.92 ± 0.03	9.7[*c]
2	9.09 ± 0.04	7.77 ± 0.04	7.8-9.2[*d]
4	6.83 ± 0.05	5.00 ± 0.12	5.0-6.6[*d]
5	6.57 ± 0.05	5.35 ± 0.03	6.5-7.4[*e]
7	6.33 ± 0.04	5.43 ± 0.01	6.11 ± 0.09[**f]
8	7.40 ± 0.03	5.97 ± 0.05	6.32 ± 0.18[**f]
9	5.73 ± 0.03	5.26 ± 0.06	<4.5[**f]
10	8.76 ± 0.07	7.63 ± 0.13	8.2[*d]
19	8.96 ± 0.06	7.99 ± 0.10	9.12 ± 0.05[*g]
33	9.97 ± 0.20	8.98 ± 0.05	9.39 ± 0.05[*g]

[a]Determined by equilibrium binding with [^{3}H]**19** (c = 2 nM) in the presence of increasing concentrations of the respective MR ligand at intact CHO-hM_2 cells; mean values ± SEM from at least 3 independent experiments (performed in triplicate). [b]Determined by (putative) equilibrium binding with [^{3}H]**33** (c = 0.5 nM) in the presence of increasing concentrations of the respective MR ligand at CHO-hM_2 cell homogenates; mean values ± SEM from at least three independent experiments (performed in triplicate). [c]Dei *et al.*[41] [d]pK_i values from equilibrium (competition) binding experiments reported in the literature (data taken from the IUPHAR/BPS database (guidetopharmacology.org, (Nov. 2016)). [e]Jakubik *et al.*[42] [f]pIC_{50} values obtained from nonlinear four-parameter logistic curve analyses of data characterizing the inhibition of [^{3}H]NMS (c = 0.2 nM) equilibrium binding at live CHO-hM_2 cells (for compound **9** *cf.* Supporting Information, Figure S4B); mean ± SEM from at least 3 independent experiments (performed in triplicate). [g]pK_i values taken from Table 1.

In order to verify a putative competitive mechanism of the allosteric M_2R modulator **8** with [^{3}H]**19** and [^{3}H]**33** at the M_2R, equilibrium competition binding studies were performed applying increasing fixed concentrations/receptor occupancies of the radioligands (Figure 8A,

8B). In the same manner, a reference experiment was performed with **8** and the orthosteric radioligand [^{3}H]NMS (Figure 8C). The control experiment with [^{3}H]NMS revealed an elevation of the lower plateau of the curves and the pIC_{50} of **8** was unaffected, indicating a non-competitive mechanism as reported previously.[30] By contrast, the lower plateau of the curves did not increase in case of [^{3}H]**19** and [^{3}H]**33**, and a rightward shift of the pIC_{50} of **8** was observed (Figure 8A and 8B). These data support a competitive mechanism[40] between the allosteric M_2R ligand **8** and the dibenzodiazepinone-type ligands **19** and **33** and, consequently, a dualsteric binding mode of **19** and **33** at the M_2R.

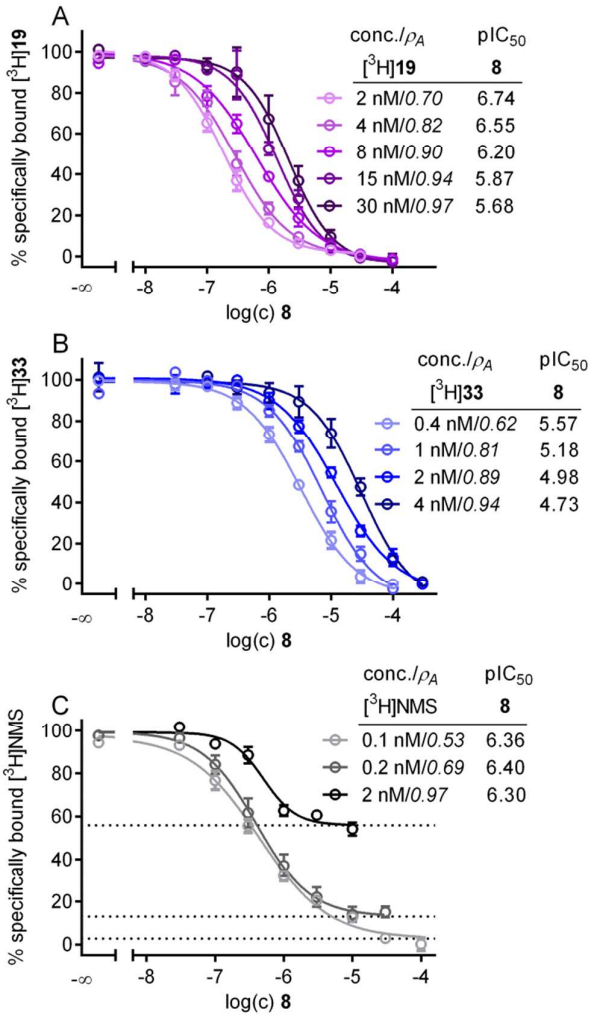

Figure 8. Effect of the allosteric MR modulator **8** on M_2R equilibrium binding of [^{3}H]**19** (K_d = 0.87 nM) (A), [^{3}H]**33** (K_d = 0.24 nM) (B) and [^{3}H]NMS (K_d = 0.09 nM) (C) using various radioligand concentrations. Experiments were performed at intact CHO-hM_2 cells (A, C) or at CHO-hM_2 cell homogenates (B). Unspecific binding was determined in the presence of atropine (500-fold excess to [^{3}H]**19**, [^{3}H]**33** or [^{3}H]NMS). Data were analyzed by four-

parameter logistic fits. In case of [^{3}H]**19** and [^{3}H]**33** increasing radioligand concentrations resulted in a parallel rightward shift of the curves, which reached 0% specific radioligand binding throughout, indicating a competitive mechanism (A, B). In contrast, curves of [^{3}H]NMS equilibrium binding obtained in the presence of increasing concentrations of **8** were not rightward-shifted, instead, the lower plateau of the curve appeared to be elevated at increased radioligand concentrations, indicating negative allosteric cooperativity between **8** and [^{3}H]NMS (C). Data represent mean values ± SEM from at least three independent experiments (performed in triplicate). ρ_A = fractional receptor occupancy

Schild-like analysis with 8 and 9 at the M_2R using [^{3}H]19 and [^{3}H]33. In order to substantiate the studies on the binding mode of [^{3}H]**19** and [^{3}H]**33** at the M_2R, saturation binding of [^{3}H]**19** and [^{3}H]**33** in the presence of the allosteric modulators **8** and **9** were performed (Figure 9). This kind of experiment is equivalent to the Schild analysis used to investigate the inhibiting effect of a receptor antagonist on the response elicited by an agonist and is considered the experiment of choice to unveil non-competitive mechanisms.[39, 40, 43] For instance, it was used to prove allosteric binding of **7** at the M_2R (radioligand: [^{3}H]NMS) and oleamide at the 5-HT_7 receptor (radioligand: [^{3}H]5-HT).[44, 45] Increasing concentrations of **8** led to a parallel rightward shift of the saturation isotherms of both, the monomeric ligand [^{3}H]**19** and the homodimeric ligand [^{3}H]**33**, resulting in linear 'Schild' regressions with a slope not different from unity (Figure 9A, 9C, Table 4), indicating a competitive mechanism between the allosteric M_2R ligand **8** and the dibenzodiazepinone-type ligands **19** and **33**. Likewise, the allosteric modulator **9**, which was co-crystalized with the M_2R bound to **6**,[23] elicited a parallel rightward shift of [^{3}H]**19** saturation isotherms, again yielding a linear 'Schild' regression with a slope not different from unity (Figure 9B, Table 4). The 'pA_2' values derived from these 'Schild' regressions were in a good accordance with the pK_i values from equilibrium competition binding studies with [^{3}H]**19** and [^{3}H]**33** as well as with reported M_2R affinities of **8** and **9** (Table 4). With regard to the fact that the dibenzodiazepinone derivatives **19** and **33** address the M_2R orthosteric binding site (see above) the results of the Schild-like analyses strongly suggested a dualsteric binding mode of **19** and **33** at the M_2R, that is, a simultaneous binding to the orthosteric site and the allosteric vestibule.

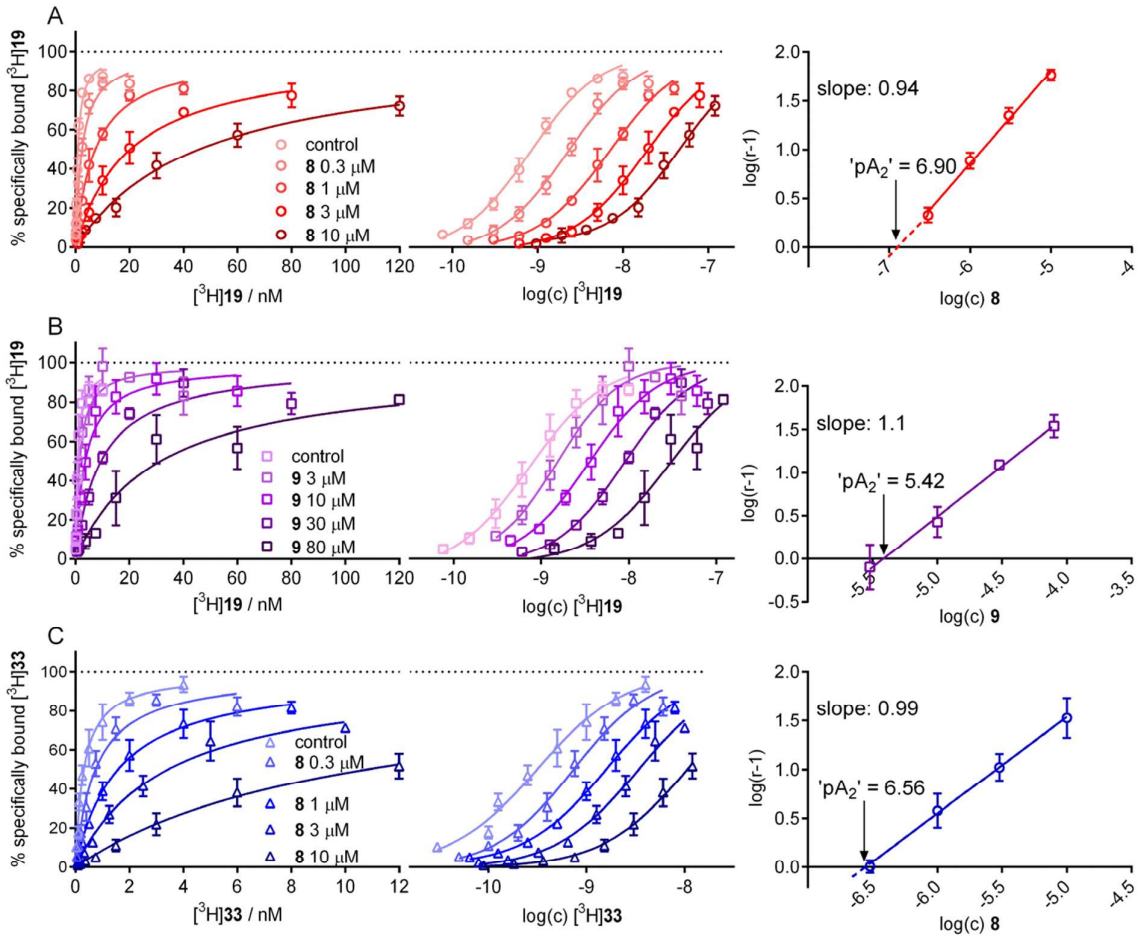

Figure 9. Saturation binding of [^{3}H]**19** in the presence of increasing concentrations of **8** (A) or **9** (B), and of [^{3}H]**33** in the presence of increasing concentrations of **8** (C). Presented are saturation isotherms of specific radioligand binding to the M_2R in linear scale (left) and semi-logarithmic scale (middle), and 'Schild' regressions (right) resulting from the rightward shifts (ΔpK_d) of the saturation isotherms (log(r−1) plotted vs. log(concentration allosteric modulator), where $r = 10^{\Delta pKd}$). The presence of the allosteric modulator (**8**, **9**) led to a parallel rightward shift of the saturation isotherms of both, the monomeric ([^{3}H]**19**) and the homodimeric ([^{3}H]**33**) radiolabeled dibenzodiazepinone derivative. In all cases the slope of the linear 'Schild' regression was nearly equal to unity indicating a competitive interaction between the radioligands and the investigated allosteric ligands. Experiments were performed at intact CHO-hM_2 cells (A, B) or at CHO-hM_2 cell homogenates (C). Data represent mean values ± SEM from at least three independent experiments (each performed in triplicate).

Table 4. Summary of M_2R binding data of the allosteric M_2R modulators **8** and **9** determined by the use of the radiolabeled dibenzodiazepinone derivatives [^{3}H]**19** and [^{3}H]**33**.

allosteric ligand	used radioligand	slope[a]	'pA_2'[b]	pK_i[c]	pK_X* or pK_B**
8	[^{3}H]**19**	0.94 ± 0.04	6.81 ± 0.02	7.39 ± 0.03	7.50*[d]
9	[^{3}H]**19**	1.1 ± 0.1	5.45 ± 0.09	5.73 ± 0.03	5.77**[e]
8	[^{3}H]**33**	0.98 ± 0.06	6.58 ± 0.01	5.91 ± 0.06	7.50*[d]

[a]Slope of the 'Schild' regression constructed based on radioligand binding data from saturation binding experiments in the presence of increasing fixed concentrations of the allosteric ligands **8** or **9**; mean values ± SEM from at least three sets of independent saturation binding experiments (performed in triplicate). The slope of the linear 'Schild' regression was not significantly different from unity ($P > 0.2$). [b]The 'pA_2' value corresponds to the X-axis intercept of the linear 'Schild' regression (*cf.* Fig. 9) and reflects the affinity of the investigated allosteric ligands. [c]pK_i values taken from Table 3. [d]Tränkle *et al*.[15] [e]Kruse *et al*.[23]

Molecular dynamics simulations. Aiming at a verification of the conclusions drawn from the experimental data by computational methods, MD simulation of the human M_2R bound to the dibenzodiazepinone derivative **19** or **33** (2 and 3 µs, respectively) were performed. Simulations were prepared by induced fit docking of **19** and **33** to the M_2R in the inactive state (*cf.* Supporting Information, Figure S9). The docking-derived orientation of **19** showed interactions of **19** with the lower part of the allosteric vestibule (Figure S9A), which was, regardless of minor conformational changes, persistent during the 2-µs simulation (Figure 10A, Figure S10 (Supporting Information)). Amino acid residues, reported to be involved in binding of the allosteric M_2R ligand **9**,[23] appeared to be in close proximity to the monomeric ligand **19** (Figure 10A). These data suggested a (partial) overlap of the binding sites of **9** and **19**, which is consistent with the results of the experiments presented in Figure 9B (Schild-like analysis). Notably, the backbone contact between the propionamide moiety in **19** and $I178^{ECL2}$ suggested that **19** reaches the extracellular surface of the M_2R.

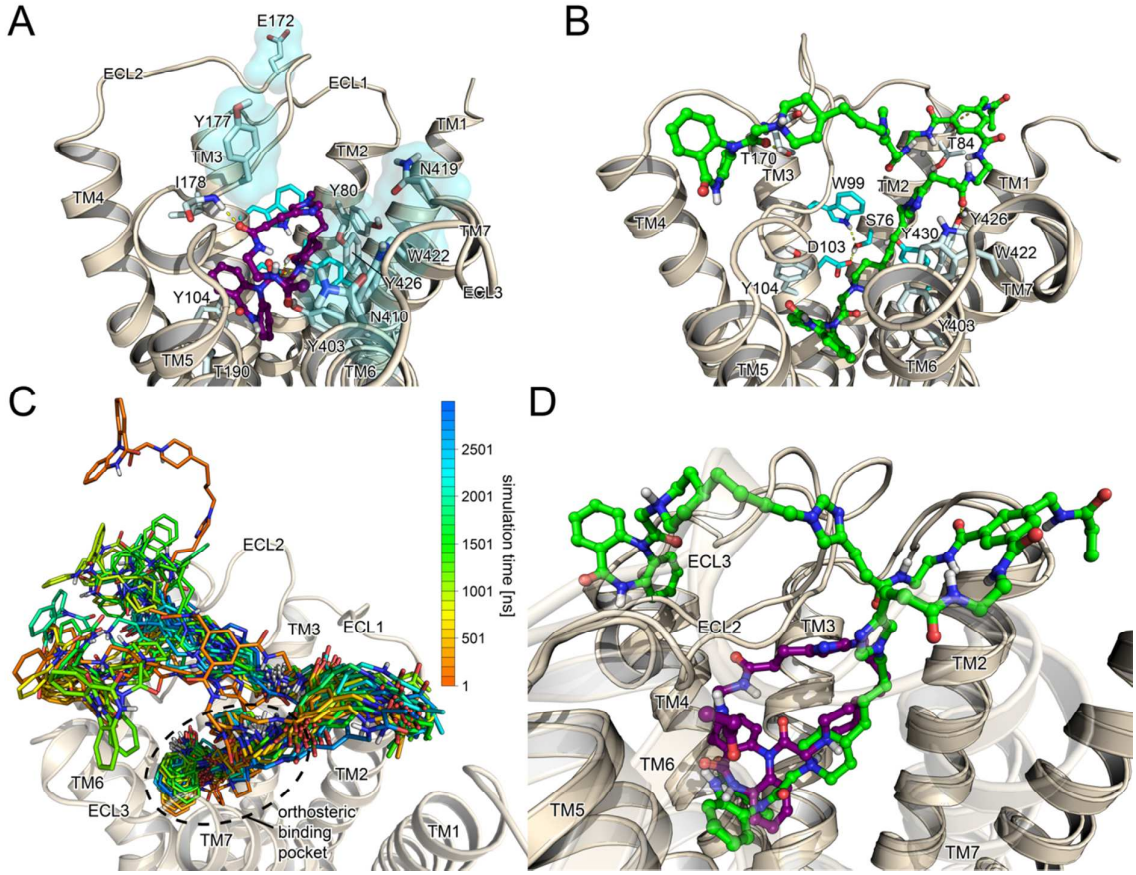

Figure 10. Molecular dynamics simulation of the human M_2R (inactive state, PDB ID 3UON) bound to the dibenzodiazepinone derivatives **19** and **33** (2 and 3 µs, respectively). (A) Cluster 1 binding pose of **19** (shown in purple). (B) Cluster 1 binding pose of **33** (shown in green). In A and B carbon atoms of amino acids constituting the $D103^{3.32}$-$W99^{3.28}$-$S76^{2.57}$-$Y430^{7.43}$ cluster are highlighted in cyan (only assigned in B). Key amino acids suggested to interact with **19** were $Y104^{3.33}$ (π-π), $I178^{ECL2}$ (HB), $T190^{5.42}$ (HB) and $Y403^{6.51}$ (HB) (A). Key amino acids suggested to interact with **33** were $T84^{2.65}$ (HB), $D103^{3.32}$ (HB), $Y104^{3.33}$ (π-π), $T170^{ECL2}$ (HB), $Y403^{6.51}$ (HB), $W422^{7.35}$ (HB) and $Y426^{7.39}$ (HB) (B). In A, amino acids reported to interact with the allosteric modulator **9**, that is $Y80^{2.61}$, $E172^{ECL2}$, $Y177^{ECL2}$, $N410^{6.58}$, $N419^{7.32}$, $W422^{7.35}$ and $Y426^{7.39}$, are surrounded by transparent cyan surface.[23] (C) Time course of the 3-µs MD simulation of the M_2R bound to **33** showing superimposed snap shots collected every 100 ns. (D) Superimposition of the cluster 1 binding poses of **19** (purple) and **33** (green). HB = hydrogen bonding.

As also observed for the monomeric compound **19,** the orientation of the orthosterically bound part of the dimeric ligand **33** varied only marginally during the 3-µs simulation, that is, it remained tightly bound to the orthosteric site. By contrast, the major part of the linker and the second dibenzodiazepinone pharmacophore in **33**, being unbound and located in the 'extracellular space' at the beginning of the simulation (*cf.* Figure S9B (Supporting

Information) and frame 1 (orange) in Figure 10C), showed a high flexibility over the first 2 μs (in part reflected by Figure 10C and Figure S11 (Supporting Information)). Strikingly, in the late phase of the simulation the flexibility of the allosterically interacting part of **33** was much lower resulting in a persistence of the predominant binding pose of **33** (represented by cluster 1, Figure 10D, Table S1 (Supporting Information)) over 1 μs (Figure 10C). A MPG1 movie file showing the entire MD simulation of **33** is available. Interestingly, Asp103$^{3.32}$, which typically forms a salt bridge with basic amine functions of MR agonists as a key interaction for receptor activation[46] showed an interaction with the dimeric compound **33**, but not with the monomeric ligand **19** (Supporting Information, Figure S12B). This was also reported for crystal structures of the M_1 and M_4 receptor in complex with an antagonist.[24] In both simulations, Asp103$^{3.32}$ formed an H-bonding network with Ser76$^{2.57}$ and Trp99$^{3.28}$, in case of the simulation with **19** additionally with Tyr430$^{7.43}$ (*cf.* Supporting Information, Figure S12A), which is characteristic of the inactive receptor conformation.[24] As anticipated, the homodimeric ligand **33** showed more 'allosteric contacts' in the simulation compared to the monomeric ligand **19**. Summarized, the results obtained from the MD simulations were consistent with the results of the aforementioned experiments, which suggested a dualsteric binding mode of the investigated tricyclic MR ligands **19** and **33**.

M_2R binding studies with 50. Compound **50**, representing the allosterically interacting part of the dualsterically binding MR ligand **19**, was investigated with respect to M_2R binding by studying its potential inhibitory effect on M_2R equilibrium binding of [^{3}H]NMS and [^{3}H]**19** at intact CHO-hM_2 cells. **50** could not 'inhibit' M_2R binding of [^{3}H]NMS and [^{3}H]**19** at concentrations below 100 μM (Supporting Information, Figure S13) suggesting that the allosteric interactions of **19** are not or only marginally responsible for the high M_2R affinity of the dualsteric ligand **19**.

Conclusion

The presented study comprises the first report on tritium-labeled dibenzodiazepinone-type, M_2R subtype-preferring MR antagonists including the comparison of a homodimeric derivative ([^{3}H]**33**) with its monomeric counterpart ([^{3}H]**19**). With K_d values below 1 nM both radioligands exhibited considerably higher M_2R affinities than the structurally related pyridobenzodiazepinone-type MR antagonist [^{3}H]**10** (K_d = 11 nM, M_2R), that was previously suggested to bind to the allosteric vestibule of the M_2R.[30] The synthesis of the radiolabeled compounds [^{3}H]**19** and [^{3}H]**33** contributed significantly to the elucidation of the M_2R binding mode of the high affinity dibenzodiazepinone derivatives **19** and **33**. The results from various binding experiments with [^{3}H]**19** and [^{3}H]**33**, in particular, saturation binding studies in the absence and in the presence of well characterized allosteric M_2R ligands (compounds **8** and **9**) (Figure 9) as well as dissociation studies at the M_2R in the presence of **8** (Figure 6B and 6D), strongly indicated that the presented type of M_2R antagonists (**19**, **33**, and presumably the reported congeners **20** and **21**, too) interact simultaneously with both the orthosteric and the 'common' allosteric binding site. Therefore, this study demonstrates that the use of radiolabeled analogs can significantly contribute to a better understanding of the binding mode of complex receptor ligands. The chemically stable dualsteric radioligands [^{3}H]**19** and [^{3}H]**33**, which could be conveniently synthesized and exhibited high M_2R affinity, represent useful tools to study their binding mode at MRs. However, whereas the monomeric ligand [^{3}H]**19** represents a new valuable molecular tool complementary to known orthosteric MR radioligands, the use of the dimeric radioligand [^{3}H]**33** to characterize the binding of non-labeled M_2R ligands is compromised by its irreversible binding at the M_2R. This work suggests dibenzodiazepinone-type MR ligands as privileged structures to develop M_2R selective antagonists according to the dualsteric ligand approach[8, 14, 17-21] by the synthesis of heterodimeric ligands comprising a linkage of the dibenzodiazepinone scaffold to reported allosteric M_2R pharmacophores as well as to newly designed allosterically interacting

moieties based on the information of MR crystal structures. With regard to the low selectivity towards the M_4R of the investigated type of MR ligands, compounds such as **19** and **33** may also represent lead structures for the development of M_4R selective ligands.

Experimental Section

General experimental conditions. Chemicals and solvents were purchased from commercial suppliers and were used without further purifications unless otherwise specified. Acetonitrile for HPLC (gradient grade) was obtained from Merck (Darmstadt, Germany). *N*-methyl scopolamine (**1**), atropine (**2**), carbachol (**3**), gallamine (**7**), **8**, **22**, **34**, **39** and **40** were purchased from Sigma-Aldrich (Deisenhofen, Germany). Oxotremorine sesquifumarate (**4**) was from MP Biomedicals (Eschwege, Germany), compound **9** was from Absource Diagnostic (Munich, Germany) and **10** was purchased from Abcam (Cambridge, UK). [^{3}H]NMS (specific activity = 80 Ci/mmol) was purchased from American Radiolabeled Chemicals Inc. (St. Louis, MO) via Hartmann Analytics GmbH (Braunschweig, Germany). The syntheses of dibenzodiazepinone derivative **30**,[32] urocanic acid derivative **48**[32] and compound **53**[47] were described previously. Xanomeline (**5**) and compound **36** were synthesized according to described procedures.[48, 49] Technical grade solvents (CH_2Cl_2, ethyl acetate, light petroleum) were distilled before use. For solvent dehydration THF and diethyl ether were distilled over sodium, and CH_2Cl_2 was distilled over P_2O_5 after predrying over $CaCl_2$. Millipore water was used throughout for the preparation of buffers and HPLC eluents. Polypropylene reaction vessels (1.5 or 2 mL) with screw cap (Süd-Laborbedarf, Gauting, Germany) were used for the synthesis of radioligands ([^{3}H]**19**, [^{3}H]**33**, [^{3}H]**47**), for small scale reactions, for the investigation of chemical stabilities (**19**, **47**) and for the preparation and storage of stock solutions. The chemical stability of **33** was investigated in a flat-bottom glass tube (40 × 8.2 mm) (Altmann Analytik GmbH, Munich, Germany), which was siliconized before use using Sigmacote (Sigma-Aldrich). Thin layer chromatography (TLC)

was performed on Merck silica gel 60 F_{254} TLC aluminum plates. Visualization was accomplished by UV irradiation (λ = 254 or 366 nm) and by staining with ninhydrin or potassium permanganate. Silica Gel 60 (40-60 μm, Merck) was used for column chromatography. A Biotage Initiator microwave synthesizer (Biotage, Uppsala, Sweden) was used for microwave driven reactions. NMR spectra were recorded on a Bruker Avance 300 (7.05 T, ^{1}H: 300.1 MHz, ^{13}C: 75.5 MHz), Bruker Avance III HD 400 (9.40 T, ^{1}H: 400 MHz, ^{13}C: 100 MHz) or a Bruker Avance III HD 600 equipped with a cryogenic probe (14.1 T ^{1}H: 600.1 MHz, ^{13}C: 150.9 MHz) (Bruker, Karlsruhe, Germany) with TMS as external standard. IR spectra were measured with a NICOLET 380 FT-IR spectrophotometer (Thermo Electron Corporation). Low-resolution mass spectrometry (MS) was performed on a Finnigan SSQ 710A instrument (CI-MS) (Thermo Finnigan, San Jose, CA). High-resolution mass spectrometry (HRMS) analysis was performed on an Agilent 6540 UHD Accurate-Mass Q-TOF LC/MS system (Agilent Technologies, Santa Clara, CA) using an ESI source. Preparative HPLC was performed with a system from Knauer (Berlin, Germany) consisting of two K-1800 pumps and a K-2001 detector. A Kinetex-XB C18 (5 μm, 250 mm × 21 mm; Phenomenex, Aschaffenburg, Germany) or an Actus Triart C18 (5 μm, 150 mm × 21 mm; YMC Europe GmbH, Dinslaken, Germany) were used as stationary phases at a flow rate of 18 mL/min. Mixtures of acetonitrile and 0.1% aq TFA and mixtures of acetonitrile and 0.1% aq ammonia, respectively, were used as mobile phase. The detection wavelength was set to 220 nm throughout. The solvent of the collected fractions was removed by lyophilization using an Alpha 2-4 LD apparatus (Martin Christ, Osterode am Harz, Germany) equipped with a RZ 6 rotary vane vacuum pump (Vacuubrand, Wertheim, Germany). Analytical HPLC analysis of compounds **19**, **33** and **47** (concentrations between 25 and 50 μM) was performed with a system from Agilent Technologies composed of a 1290 Infinity binary pump equipped with a degasser, a 1290 Infinity autosampler, a 1290 Infinity thermostated column compartment, a 1260 Infinity diode array detector, and a 1260 Infinity fluorescence detector.

A Kinetex-XB C18 (2.6 µm, 100 × 3 mm; Phenomenex) served as stationary phase at a flow rate of 0.5 mL/min except for the analysis of **50**. Mixtures of 0.04% aq TFA (A) and acetonitrile (B) were used as mobile phase. The following linear gradient was applied: 0-20 min: A/B 90:10-68:32, 20-22 min: 68:32-5:95, 22-28 min: 5:95. Analytical HPLC analysis of compound **50** was performed using an Actus Triart C18 (3 µm, 150 × 2 mm; YMC Europe) as stationary, and mixtures of 0.1% aq ammonia (C) and acetonitrile (B) as mobile phase (flow rate: 0.5 mL/min). The following linear gradient was applied: 0-10 min: C/B 95:5-90:10, 10-20 min: 90:10-10:90, 20-28 min: 10:90. For all analytical HPLC runs the oven temperature was set to 25 °C, the injection volume was 20 µL and detection was performed at 220 nm. Melting points were determined with a Büchi 510 apparatus (Büchi, Essen, Germany) and are uncorrected.

Annotation concerning the NMR spectra (^{1}H, ^{13}C) of the dibenzodiazepinone derivatives (**31**, **33**, **37**, **38**, **46**, **47**): due to a slow rotation about the exocyclic amide group on the NMR time scale, two isomers (ratios provided in the experimental protocols) were evident in the ^{1}H- and ^{13}C-NMR spectra.

Compound characterization. New organic compounds were characterized by ^{1}H- and ^{13}C-NMR spectroscopy, HRMS and melting point (if applicable). In addition, the target compounds **31**, **33**, **46**, **47, 50** and **52** were characterized by 2D-NMR spectroscopy (^{1}H-COSY, HSQC, HMBC) and RP-HPLC analysis. Furthermore, IR spectra were acquired for the homodimeric ligands **33** and **47**. The purity of final compounds, determined by RP-HPLC (220 nm), was ≥97% throughout (chromatograms shown in the Supporting Information).

Chemistry: experimental protocols and analytical data (compounds 31, 33, 35, 37, 38, 46, 47, 49, 50 and 52)

5-(Aminomethyl)-N^1,N^3-bis(2-(3-(1-(4-(1-(2-oxo-2-(11-oxo-10,11-dihydro-*5H*-dibenzo[*b,e*][1,4]diazepin-5-yl)ethyl)piperidin-4-yl)butyl)-1H-imidazol-4-yl)propanamido)ethyl) isophthalamide pentakis(hydrotrifluoroacetate) (31). HOBt (39 mg, 0.29 mmol), TBTU (188 mg, 0.584 mmol) and DIPEA (132 µL, 0.75 mmol) were added to a solution of **29** (43 mg, 0.15 mmol) in DMF and the mixture was stirred at rt for 15 min. Amine **30** (tris(hydrotrifluoroacetate))[32] was added and stirring was continued at 60 °C for 3 h. The volatiles were removed under reduced pressure, the residue was dissolved in CH_2Cl_2/TFA/H_2O 10:10:1 (v/v/v, 8 mL) and the mixture was stirred at rt for 2 h followed by evaporation of the volatiles. Purification by preparative HPLC (column: Kinetex-XB C18, gradient: 0-25 min: 0.1% aq TFA/acetonitrile 90:10-60:40, t_R = 16 min) yielded **31** as a white fluffy solid (89 mg, 0.048 mmol, 32%). Ratio of configurational isomers evident in the NMR spectra: ca 1.6:1. ^{1}H-NMR (600 MHz, MeOH-d_4): δ (ppm) 1.30-1.36 (m, 8H), 1.40-1.58 (m, 6H), 1.80-1.98 (m, 8H), 2.60 (t, 4H, *J* 7.2 Hz), 2.85-2.94 (m, 2H), 2.97 (t, 4H, *J* 7.2 Hz), 3.00-3.11 (m, 2H), 3.41 (t, 4H, *J* 6.2 Hz), 3.43-3.49 (m, 2H), 3.50 (t, 4H, *J* 6.1 Hz), 3.73 (d, 3H, *J* 16.4 Hz), 3.80 (d, 1H, *J* 16.6 Hz), 4.15 (t, 4H, *J* 7.3 Hz), 4.24 (s, 2H), 4.41 (d, 1H, *J* 16.6 Hz), 4.45 (d, 1H, *J* 16.6 Hz), 7.22-7.42 (m, 7H), 7.44-7.56 (m, 4H), 7.59-7.72 (m, 4H), 7.75 (t, 1H, *J* 1.6 Hz), 7.90 (d, 1H, *J* 8.1 Hz), 7.96 (d, 1H, *J* 7.9 Hz), 8.06 (d, 2H, *J* 1.5 Hz), 8.28 (t, 1H, *J* 1.7 Hz), 8.80 (d, 2H, *J* 1.5 Hz). ^{13}C-NMR (150.9 MHz, MeOH-d_4): δ (ppm) 21.51, 24.17, 30.39, 31.08, 34.26, 34.88, 36.00, 40.08, 40.93, 43.79, 50.34, 54.87, 55.23, 58.08, 119.78, 123.08, 123.65, 126.85, 127.52, 127.89, 128.48, 128.87, 129.44, 130.11, 130.55, 130.88, 131.21, 131.71, 131.87, 131.95, 132.34, 133.00, 133.40, 134.57, 134.92, 135.26, 135.47, 135.52, 135.72, 137.02, 141.00, 142.67, 164.98, 165.48, 168.81, 168.84, 174.02. HRMS (ESI): *m/z* $[M+4H]^{4+}$ calcd. for $[C_{73}H_{91}N_{15}O_8]^{4+}$ 326.4289, found 326.4305. RP-HPLC (220 nm): 98% (t_R = 11.7 min, *k* = 11.6). $C_{73}H_{87}N_{15}O_8 \cdot C_{10}H_5F_{15}O_{10}$ (1302.60 + 570.12).

N^1,N^3-Bis(2-(3-(1-(4-(1-(2-oxo-2-(11-oxo-10,11-dihydro-5H-dibenzo[b,e][1,4]diazepin-5-yl)ethyl)piperidin-4-yl)butyl)-1H-imidazol-4-yl)propanamido)ethyl)-5-(propionamidomethyl)isophthalamide tetrakis(hydrotrifluoroacetate) (33). Succinimidyl proprionate (**32**) (3.28 mg, 19 μM) was added to a solution of **31** (30 mg, 0.016 mM) and DIPEA (22 μL, 0.128 mmol) in anhydrous DMF (0.45 mL) and the mixture was stirred at rt for 45 min. 10% aq TFA (1 mL) was added and the product was purified by preparative HPLC (column: Kinetex-XB C18, gradient: 0-25 min: 0.1% aq TFA/acetonitrile 90:10-60:40, t_R = 18 min). **33** was obtained as a white fluffy solid (28 mg, 0.015 mmol, 95%). IR (KBr): 3310, 3130, 3065, 2940, 2865, 1665, 1550, 1505, 1460, 1365, 1200, 1135, 800, 720 cm^{-1}. Ratio of configurational isomers evident in the NMR spectra: ca 1.7:1. ^{1}H-NMR (600 MHz, MeOH-d_4): δ (ppm) 1.15 (t, 3H, *J* 7.6 Hz), 1.30-1.33 (m, 8H), 1.38-1.57 (m, 6H), 1.77-1.98 (m, 8H), 2.30 (q, 2H, *J* 7.6 Hz), 2.59 (t, 4H, *J* 7.1 Hz), 2.88-2.95 (m, 2H), 2.97 (t, 4H, *J* 7.1 Hz), 3.01-3.08 (m, 2H), 3.40 (t, 4H, *J* 6.0 Hz), 3.42-3.47 (m, 2H), 3.48 (t, 4H, *J* 6.0 Hz), 3.73 (d, 3H, *J* 16.3 Hz), 3.80 (d, 1H, *J* 16.6 Hz), 4.13 (t, 4H, *J* 7.3 Hz), 4.41 (d, 1H, *J* 16.7 Hz), 4.44 (s, 2H), 4.45 (d, 1H, *J* 16.6 Hz), 7.24-7.40 (m, 7H), 7.45-7.55 (m, 4H), 7.60-7.71 (m, 4H), 7.74 (t, 1H, *J* 1.6 Hz), 7.86 (d, 2H, *J* 1.6 Hz), 7.90 (d, 1H, *J* 8.1 Hz), 7.96 (d, 1H, *J* 7.8 Hz), 8.12 (t, 1H, *J* 1.7 Hz), 8.77 (d, 2H, *J* 1.5 Hz). ^{13}C-NMR (150.9 MHz, MeOH-d_4): δ (ppm) 10.39, 21.50, 24.15, 30.13, 30.38, 31.06, 34.25, 34.81, 36.00, 40.14, 40.93, 43.67, 50.33, 54.90, 55.31, 58.02, 119.77, 123.08, 123.65, 126.22, 126.84, 127.52, 127.88, 128.48, 128.88, 129.44, 130.11, 130.15, 130.55, 130.89, 131.21, 131.71, 131.95, 132.35, 133.00, 133.40, 134.57, 134.91, 135.24, 135.42, 135.72, 136.38, 137.02, 141.61, 142.67, 165.48,169.36, 174.03, 177.21. HRMS (ESI): *m/z* $[M+4H]^{4+}$ calcd. for $[C_{73}H_{95}N_{15}O_9]^{4+}$ 340.4354, found 340.4367. RP-HPLC (220 nm): 98% (t_R = 13.4 min, *k* = 13.6). $C_{73}H_{91}N_{15}O_9 \cdot C_8H_4F_{12}O_8$ (1358.66 + 456.09).

4-(Piperidin-4-yl)butan-1-ol (35).[50] Under an atmosphere of argon piperidine derivative **34** (800 mg, 3.9 mmol) was suspended in anhydrous THF (15 mL) and the mixture was cooled in an ice-bath. $LiAlH_4$ (365 mg, 9.6 mmol) was added portionwise over a period of 10 min. The resulting suspension was stirred at 0 °C for 1 h and under reflux for 12 h. The mixture was cooled to rt and 20% aq NaOH (w/w, 10 mL) was added and the suspension was vigorously stirred for 1 h. Solid material was removed by filtration through a pad of celite and the volatiles of the filtrate were removed under reduced pressure to yield **35** as a pale yellow oil (539 mg, 3.4 mmol, 89%), which was used without purification. HRMS (ESI): *m/z* $[M+H]^+$ calcd. for $[C_9H_{20}NO]^+$ 158.1540, found 158.1541. $C_9H_{19}NO$ (157.26).

5-(2-(4-(4-Hydroxybutyl)piperidin-1-yl)acetyl)-5,10-dihydro-11H-dibenzo[b,e][1,4] diazepin-11-one (37). Freshly grained K_2CO_3 (3.19 g, 6.9 mmol) was added to a solution of **35** (0.91 g, 5.8 mmol) and dibenzodiazepinone derivative **36**[51] in acetonitrile (30 mL) and the mixture was vigorously stirred under reflux for 5 h. Solid material was removed by filtration, the filtrate collected and the volatiles evaporated under reduced pressure. The residue was dissolved in EtOAc (30 mL) and the solution was washed with H_2O (3 × 30 mL). The organic phase was dried over Na_2SO_4 and the solvent was removed under reduced pressure. Purification by column chromatography (eluent: CH_2Cl_2/MeOH/NH_3 (7 M in MeOH) 100:5:1 (R_f = 0.3)) afforded **37** as a colorless glass (1.0 g, 2.5 mmol, 43%). Ratio of configurational isomers evident in the NMR spectra: ca 2.1:1. ^{1}H-NMR (300 MHz, MeOH-d_4): δ (ppm) 0.99-1.41 (m, 7H), 1.42-1.70 (m, 4H), 1.81-2.12 (m, 2H), 2.46-2.70 (m, 1H), 2.83 (t, 1H, *J* 11.4 Hz*),* 2.97-3.29 (m, 2H), 3.52 (t, 2H, *J* 6.5 Hz), 7.16-7.73 (m, 7H), 7.88 (t, 1H, *J* 9.3 Hz). ^{13}C-NMR (150 MHz, MeOH-d_4): δ (ppm) 24.05, 30.16, 32.90, 33.84, 36.42, 37.37, 54.82, 54.99, 60.96, 62.91, 122.95, 126.56, 126.94, 127.76, 128.92, 129.46, 129.87, 130.55, 132.01, 132.17, 134.27, 134.68, 135.92, 143.83. HRMS (ESI): *m/z* $[M+H]^+$ calcd. for $[C_{24}H_{30}N_3O_3]^+$ 408.2282, found 408.2290. $C_{24}H_{29}N_3O_3$ (407.51).

5-(2-(4-(4-Bromobutyl)piperidin-1-yl)acetyl)-5,10-dihydro-11H-dibenzo[b,e][1,4]diazepin-11-one (38). In a three-necked round-bottom flask compound **37** (200 mg, 0.49 mmol) and triphenylphosphine (386 mg, 1.47 mmol) were dissolved in CH_2Cl_2 (5 mL) under an atmosphere of argon and the mixture was cooled to −5°C. Tetrabromomethane (1.058 g, 3.19 mmol) in CH_2Cl_2 (10 mL) was added dropwise to over a period of 10 min and the mixture was stirred at 0 °C for 5 h followed by washing with H_2O (2 x 10 mL) and brine (1 x 10 mL). The organic phase was dried over Na_2SO_4 and the solvent was removed under reduced pressure. The residue was subjected to column chromatography (eluent: light petroleum/acetone/25% aq NH_3 (83:16:1 (R_f = 0.5)) to give **38** as a white solid (180 mg, 79%). Ratio of configurational isomers evident in the NMR spectra: ca 2:1. ^{1}H-NMR (600 MHz, MeOH-d_4): δ (ppm) 0.83-1.33 (m, 7H), 1.33-1.67 (m, 4H), 1.86-2.05 (m, 2H), 2.45-2.71 (m, 1H), 2.85 (t, 1H, *J* 12.0 Hz), 2.98-3.30 (m, 2H), 3.42 (t, 2H, *J* 6.7 Hz), 7.18-7.72 (m, 7H), 7.88 (t, 1H, *J* 9.5 Hz). ^{13}C-NMR (150 MHz, MeOH-d_4): δ (ppm) 26.31, 32.83, 34.13, 34.40, 36.27, 36.55, 54.89, 54.94, 60.93, 61.29, 123.00, 126.95, 127.76, 128.89, 129.46, 130.56, 131.93, 132.16, 133.33, 133.75, 133.79, 134.25, 135.89, 143.80. HRMS (ESI): m/z $[M+H]^+$ calcd. for $[C_{24}H_{29}BrN_3O_2]^+$ 470.1438, found: 470.1437. $C_{24}H_{28}BrN_3O_2$ (470.41).

5,5'-(2,2'-(((6-Amino-1,4-diazepane-1,4-diyl)bis(butane-4,1-diyl))bis(piperidine-4,1-diyl))bis(acetyl))bis(5,10-dihydro-11*H*-dibenzo[*b,e*][1,4]diazepin-11-one) pentakis(hydrotrifluoroacetate) (46). Dibenzodiazepinone **38** (60 mg, 0.13 mmol) and homopiperazine **45** (13 mg, 0.061 mmol) were dissolved in acetonitrile (1.5 mL). Freshly grained K_2CO_3 (38 mg, 0.24 mmol) was added and the mixture was stirred and heated in a microwave reactor at 120 °C for 1.5 h. The solvent was removed under reduced pressure and the residue was taken up in EtOAc (5 mL) followed by washing with H_2O (3 × 5 mL). The organic phase was dried over Na_2SO_4 and the volatiles were removed *in vacuo*. The residue

was dissolved in a mixture formed by CH_2Cl_2/TFA/H_2O 10:10:1 (v/v/v, 3 mL) and the solution was stirred at rt for 3 h. The volatiles were evaporated and the residue was taken up in DMF/0.1% aq TFA 1:1 (v/v, 3 mL) and subjected to preparative HPLC (column: Kinetex-XB C18, gradient: 0-25 min: 0.1% aq TFA/acetonitrile 90:10-50:50, t_R = 16 min) to yield **46** as a white fluffy solid (33 mg, 0.023 mmol, 37%). Ratio of configurational isomers evident in the NMR spectra: ca 1.5:1. ^{1}H-NMR (600 MHz, MeOH-d_4): δ (ppm) 1.26-1.57 (m, 14H), 1.57-1.68 (m, 4H), 1.85-2.02 (m, 4H), 2.88-2.98 (m, 6H), 3.00-3.08 (m, 2H), 3.11-3.20 (m, 2H), 3.23-3.30 (m, 4H), 3.36-3.50 (m, 4H), 3.68-3.89 (m, 5H), 4.40 (d, 1.2H, *J* 16.8 Hz), 4.44 (d, 0.8H, *J* 16.8 Hz), 7.24-7.41 (m, 5H), 7.45-7.56 (m, 4H), 7.60-7.71 (m, 4H), 7.75 (t, 1H, *J* 7.7 Hz), 7.90 (d, 1H, *J* 8.4 Hz), 7.97 (d, 1H, *J* 7.8 Hz). ^{13}C-NMR (150.9 MHz, MeOH-d_4): δ (ppm) 24.90, 26.54, 30.58, 34.47, 36.50, 53.81, 55.11, 55.47, 55.96, 58.08, 58.19, 59.83, 123.23, 123.80, 127.00, 127.67, 128.02, 128.63, 129.03, 129.60, 130.26, 130.70, 131.04, 131.36, 131.86, 132.12, 132.50, 133.16, 134.72, 135.09, 135.61, 136.87, 137.19, 141.16, 142.83, 155.56 165.11, 165.59, 168.72, 168.98. HRMS (ESI): m/z $[M+3H]^{3+}$ calcd. for $[C_{53}H_{70}N_9O_4]^{3+}$ 298.8511, found: 298.8520. RP-HPLC (220 nm): 96% (t_R = 12.5 min, k = 12.5). $C_{53}H_{67}N_9O_4 \cdot C_{10}H_5F_{15}O_{10}$ (894.18 + 570.12).

***N*-(1,4-Bis(4-(1-(2-oxo-2-(11-oxo-10,11-dihydro-5*H*-dibenzo[*b,e*][1,4]diazepin-5-yl)ethyl)piperidin-4-yl)butyl)-1,4-diazepan-6-yl)propionamide tetrakis(hydrotrifluoroacetate) (47).** Succinimidyl proprionate **32** (2.7 mg, 0.015 mmol) was added to a solution of amine **46** (16 mg, 0.011 mmol) and DIPEA (15 µL, 0.087 mmol) in anhydrous DMF (400 µL) and the mixture was stirred at rt for 1.5 h. 10% aq TFA (20 µL) was added and the mixture was subjected to preparative HPLC (column: Kinetex-XB C18, gradient: 0-25 min: 0.1% aq TFA/acetonitrile 90:10-50:50, t_R = 16 min) to yield **47** as a white fluffy solid (11.5 mg, 0.008 mmol, 72%). IR (KBr): 3435, 3060, 2945, 2865, 1680, 1505, 1460, 1365, 1200, 1130, 800, 720 cm^{-1}. Ratio of configurational isomers evident in the NMR

spectra: ca 1.5:1. ^{1}H-NMR (600 MHz, MeOH-d_4): δ (ppm) 1.11 (t, 3H, *J* 7.7 Hz), 1.28-1.58 (m, 14H), 1.66 (m, 4H), 1.86-2.01 (m, 4H), 2.24 (q, 2H, *J* 7.6 Hz), 2.93 (m, 2H), 3.00-3.08 (m, 6H), 3.32-3.39 (m, 4H), 3.40-3.50 (m, 6H), 3.69-3.77 (m, 3H), 3.80 (d, 1H, *J* 16,7 Hz), 4.31-4.37 (m, 1H), 4.40 (d, 1.2H, *J* 16.7 Hz), 4.44 (d, 0.8H, *J* 16.7 Hz), 7.23-7.42 (m, 5H), 7.45-7.57 (m, 4H), 7.60-7.72 (m, 4H), 7.75 (t, 1H, *J* 7.7 Hz), 7.90 (d, 1H, *J* 8.2 Hz), 7.97 (d, 1H, *J* 7.8 Hz). ^{13}C-NMR (150.9 MHz, MeOH-d_4): δ (ppm) 10.03, 24.60, 26.08, 29.86, 30.43, 34.32, 36.25, 52.93, 54.90, 54.96, 55.32, 57.59, 57.95, 58.04, 59.28, 123.08, 123.64, 126.85, 127.50, 127.86, 128.47, 128.87, 129.43, 130.11, 130.55, 130.88, 131.22, 131.71, 131.97, 132.35, 133.01, 133.40, 134.57, 134.93, 135.45, 135.72, 137.04, 141.00, 142.66, 165.43, 168.56, 168.81, 176.89. HRMS (ESI): m/z $[M+3H]^{3+}$ calcd. for $[C_{56}H_{74}N_9O_5]^{3+}$ 317.5266, found: 317.5273. RP-HPLC (220 nm): 98% (t_R = 12.8 min, *k* = 12.9). $C_{56}H_{71}N_9O_5 \cdot C_8H_4F_{12}O_8$ (950.24 + 456.09).

_N_-(2-Aminoethyl)-3-(1_H_-imidazol-4-yl)propanamide bis(hydrotrifluoroacetate) (49) Urocanic acid derivative **48**[32] (300 mg, 1.07 mmol) was dissolved in MeOH/TFA 1:1 (v/v, 8 mL) and a 10% Pd/C catalyst (30 mg) was carefully added under an atmosphere of argon. The mixture was stirred in an autoclave under an atmosphere of hydrogen at 7.9 atm at rt for 12 h. The catalyst was removed by filtration through a pad of celite and the volatiles were evaporated to yield **49** as colorless oil (299 mg, 1.01 mmol, 95%), which was used without further purification. ^{1}H-NMR (300 MHz, MeOH-d_4): δ (ppm) 2.65 (t, 2H, *J* 7.3 Hz), 2.98-3.09 (m, 4H), 3.46 (t, 2H, *J* 6.0 Hz), 7.31 (br s, 1H), 8.78 (d, 1H, *J* 1.4 Hz). ^{13}C-NMR (75 MHz, MeOH-d_4): δ (ppm) 21.15, 34.97, 38.32, 40.85, 117.10, 134.68, 134.78, 175.05. HRMS (ESI): *m/z* $[M+H]^+$ calcd. for $[C_8H_{16}N_4O_5]^+$ 183.1241, found: 183.1245. $C_8H_{15}N_4O_5 \cdot C_4H_2F_6O_2$ (182.23 + 228.04).

3-(1*H*-Imidazol-4-yl)-*N*-(2-propionamidoethyl)propanamide (50) A solution of succinimidyl proprionate **32** (23 mg, 0.134 mmol) in DMF (0.1 mL) was added to a solution of **49** (110 mg, 0.27 mmol) and DIPEA (0.234 mL, 1.34 mmol) in DMF (0.5 mL) and the mixture was stirred at rt for 30 min. 32% aq NH_3 (0.15 mL) and H_2O (3 mL) were added and the mixture was subjected to preparative HPLC (column: Actus Triart C18, gradient: 0-10 min: 0.1% aq NH_3/acetonitrile 95:5, 10-20 min: 95:5-88:12, t_R = 10 min) to afford **50** as a white solid (27.5 mg, 0.115 mmol, 43%). ^{1}H-NMR (400 MHz, MeOH-d_4): δ (ppm) 1.11 (t, 3H, *J* 7.6 Hz), 2.19 (q, 2H, *J* 7.6 Hz), 2.49 (t, 2H, *J* 7.6 Hz), 2.87 (t, 2H, *J* 7.6 Hz), 3.25 (m, 4H), 6.79 (br s, 1H), 7.56 (d, 1H, *J* 1.2 Hz). ^{13}C-NMR (100 MHz, MeOH-d_4): δ (ppm) 10.37, 23.93, 30.18, 36.86, 39.99, 40.05, 117.2, 135.93, 137.8, 175.46, 177.32. HRMS (ESI): *m/z* $[M+H]^+$ calcd. for $[C_{11}H_{19}N_4O_2]^+$ 239.1503, found: 239.1507. RP-HPLC (220 nm): 99% (t_R = 8.0 min, *k* = 3.0). $C_{11}H_{18}N_4O_2$ (238.29).

5,5'-(2,2'-(Piperazine-1,4-diyl)bis(acetyl))bis(5,10-dihydro-11*H*-dibenzo[*b,e*][1,4]diazepin-11-one) bis(hydrotrifluoroacetate) (**52**) Dibenzodiazepinone **36** (100 mg, 0.35 mmol) and piperazine (**51**) (14 mg, 0.16 mmol) were dissolved in acetonitrile (2 mL). Freshly grained K_2CO_3 (88 mg, 0.64 mmol) was added and the suspension was stirred in a microwave reactor at 130 °C (approx. 4 bar) for 30 min. Insoluble material was removed by filtration, the volatiles were evaporated and the residue subjected to preparative HPLC (column: Kinetex-XB C18, gradient: 0-25 min: 0.1% aq TFA/acetonitrile 15:85-55:45, t_R = 16 min) to yield **52** as a white fluffy solid (28 mg, 0.034 mmol, 20%). Four isomers were evident in the ^{1}H- and ^{13}C-NMR spectrum and two isomers were evident by RP-HPLC analysis (ratio 1:1). HRMS analysis revealed a uniform sample with respect to the molecular formula. ^{1}H-NMR (600 MHz, MeOH-d_4): δ (ppm) 2.55-3.18 (m, 8H), 3.43-3.56 (m, 1H), 3.56-3.65 (m, 1H), 3.65-3.72 (m, 0.5H), 3.72-3.84 (m, 0.5H), 3.86-3.98 (m, 0.5H), 4.05-4.16 (m, 0.5H) 7.22-7.39 (m, 5H), 7.40-7.53 (m, 4H), 7.53-7.75 (m, 5H), 7.84-7.98 (m, 2H). ^{13}C-NMR (150.9

MHz, MeOH-d_4): δ (ppm). 51.52, 52.08, 52.27, 52.80, 58.19, 58.48, 58.91, 59.46, 123.17, 123.52, 123.63, 123.68, 126.94, 127.49, 127.58, 127.75, 127.87, 128.72, 128.79, 129.04, 129.80, 129.88, 130.02, 130.11, 130.35, 130.44, 130.56, 130.81, 131.06, 131.44, 131.61, 132.35, 132.40, 132.48, 132.65, 134.18, 134.63, 135.19, 135.29, 135.53, 135.76, 135.92, 137.13, 142.44, 143.04, 143.24, 166.99, 168.14, 168.96, 169.14, 169.47. HRMS (ESI): m/z $[M+H]^+$ calcd. for $[C_{34}H_{31}N_6O_4]^+$ 587.2402, found: 587.2423. RP-HPLC (220 nm): 98% (t_R = 15.4, 15.6 min, k = 15.7, 15.9) $C_{34}H_{30}N_6O_4 \cdot C_4H_2F_6O_2$ (586.65 + 228.04).

Investigation of the chemical stability. The chemical stability of **19**, **33** and **47** was investigated in PBS (pH 7.4) at 22 ± 1 °C. The incubation was started by the addition of 2 µL of a 10 mM solution of **19**, **33** or **47** to PBS (198 µL) to yield a final concentration of 100 µM. After 0, 24 and 48 h, aliquots (20 µL) were taken and added to acetonitrile/1% aq TFA 2:8 (v/v, 20 µL). The resulting solutions were analyzed by RP-HPLC (analytical HPLC system and conditions see general experimental conditions; t_R: 8.8 min (**19**), 13.5 min (**33**), 12.8 min (**47**)).

Synthesis of the radioligands [^{3}H]19, [^{3}H]33 and [^{3}H]47. The tritiated dibenzodiazepinone derivatives [^{3}H]**19**, [^{3}H]**33** and [^{3}H]**47** were prepared by [^{3}H]propiolynation of the amino-functionalyzed precursors **30**, **31** and **46**, respectively, using a reported protocol with modifications.[52] A solution of succinimidyl [2,3-^{3}H]-proprionate ([^{3}H]**32**) (specific activity: 80 Ci/mmol; from Moravek, Brea, CA, via Hartmann Analytics, Braunschweig, Germany) (for [^{3}H]**19** and [^{3}H]**47**: 2.5 mCi, 5.5 µg, 31.25 nmol (each), for [^{3}H]**33**: 2 mCi, 4.4 µg, 25 nmol) in hexane/EtOAc 9:1 was transferred into a 1.5-mL reaction vessel with a screw cap and the volatiles were evaporated in a vacuum concentrator (ca 30 min at about 30 °C). A solution of the precursor molecule (**30**: 411 µg, 0.76 µmol; **31**: 870 µg, 0.46 µmol; **46**: 400 µg, 0.27 µmol) in DMF/DIPEA 50:1 (v/v, 55 µL) was added and the mixture was shaken at rt

for 45 min. In case of [^{3}H]**47** the excess of precursor **46** was 'quenched' by 4-fluorobenzoylation. For that purpose succinimidyl ester **53** (250 µg, 1.05 µmol) was added to the mixture and shaken at rt for one additional hour. After completed incubation and 'precursor quenching', 2% aq TFA (90 µL) and H_2O/acetonitrile 3:1 (v/v, 85 µL) were added. [^{3}H]**19**, [^{3}H]**33** and [^{3}H]**47** were purified using an analytical HPLC system (Waters, Eschborn, Germany) consisting of two 510 pumps, a pump control module, a 486 UV/vis detector, and a Flow-one Beta series A-500 radiodetector (Packard, Meriden, CT). A Luna C18 (3 µm, 150 mm × 4.6 mm, Phenomenex, Aschaffenburg, Germany) was used as stationary phase at a flow rate of 0.8 mL/min. Mixtures of 0.05% aq TFA (A) and acetonitrile containing 0.04% TFA (B) were used as mobile phase. The following linear gradients were applied: [^{3}H]**19** and [^{3}H]**33**, 0-20 min: A/B 90:10-68:32, 20-30 min: 68:32-5:95, 30-38 min: 5:95, t_R = 16.4 and 20.0 min, respectively); [^{3}H]**47**, 0-20 min: A/B 90:10-75:25, 20-25 min: 75:25, 25-27 min: 75:25-5:95, 27-35 min: 5:95, t_R = 24.7 min). For each radioligand, two HPLC runs (UV detection: 220 nm; no radiometric detection) were performed. Each radioligand was collected in a 2-mL reaction vessel with screw cap. The volumes of the combined eluates were reduced in a vacuum concentrator to 600 µL and EtOH (600 µL) was added. The solutions were transferred into 3-mL borosilicate glass vials with conical bottom (Wheaton NextGen 3 mL V-vials). The 2-mL reaction vessels were rinsed twice with EtOH/water 1:1 (v/v, various volumes), and the washings were transferred to the 3-mL glass vials to obtain tentative stocks with volumes of 1000 µL ([^{3}H]**19**, [^{3}H]**33**) or 1200 µL ([^{3}H]**47**). For the quantification, a five-point or four-point calibration was performed with the corresponding 'cold' forms **19** (0.1, 0.2, 0.35, 0.5, 0.75 µM), **33** (0.2, 0.4, 0.7, 1, 1.5 µM) and **47** (0.1, 0.2, 0.5, 1 µM) (injection volume throughout 100 µL, UV detection at 220 nm) using the aforementioned HPLC system and conditions (in case of [^{3}H]**47** the linear gradient was modified: 0-20 min: A/B 90:10-69:31, 20-30 min: 69-31:5:95, 30-38 min: 5:95, t_R = 19.9 min). Aliquots of the tentative stock solutions ([^{3}H]**19**: 2.2 µL, [^{3}H]**33**: 2.2 µL, [^{3}H]**47**: 2 µL) were added to 0.05% aq

TFA/acetonitrile 9:1 (v/v; 127.8 and 128 µL, respectively), 100 µL of the resulting solutions were analyzed by HPLC, and five times 2 µL were counted in 3 mL of Rotiszint eco plus (Carl Roth, Karlsruhe, Germany) with a LS 6500 liquid scintillation counter (Beckman-Coulter, Munich, Germany). These analyses were repeated. The molarities of the tentative stock solutions were calculated from the mean of the peak areas and the linear calibration curves. In order to determine the radiochemical purities and to confirm the chemical identities, solutions (100 µL) of [^{3}H]**19** (0.23 µM), [^{3}H]**33** (0.20 µM) and [^{3}H]**47** (0.20 µM) spiked with **19** (5 µM), **33** (5 µM) and **47** (3 µM), respectively, were analyzed by HPLC using the conditions as for the quantification and additionally radiometric detection (flow rate of the liquid scintillator (Rotiscint eco plus/acetonitrile (85:15 v/v): 4.0 mL/min). For all radioligands the radiochemical purity was 99%. For [^{3}H]**19** and [^{3}H]**33** this analysis was repeated after 1 year of storage at −20 °C, whereas in case of [^{3}H]**47** it was repeated after 9 months of storage at −20 °C (radiochemical purities: [^{3}H]**19**, 96%; [^{3}H]**33**, 97%; [^{3}H]**47**, 96%). Calculated specific activities: [^{3}H]**19**, 2.96 TBq/mmol (72.7 Ci/mmol); [^{3}H]**33**, 1.81 TBq/mmol (49.0 Ci/mmol); [^{3}H]**47**, 2.19 TBq/mmol (59.3 Ci/mmol). The final activity concentration was adjusted to 27.75 MBq/mL ([^{3}H]**19**) or 18.5 MBq/mL ([^{3}H]**33**, [^{3}H]**47**) by the addition of H_2O/EtOH 1:1 (v/v) resulting in molarities of 10.3 µM ([^{3}H]**19**), 10.2 µM ([^{3}H]**33**) and 8.44 µM ([^{3}H]**47**). Radiochemical yields: [^{3}H]**19**, 36.0 MBq, 39%; [^{3}H]**33**, 24.0 MBq, 32%; [^{3}H]**47**, 34.7 MBq, 38%.

Cell Culture and preparation of cell homogenates. CHO-K9 cell lines stably transfected with the human M_1-M_5 muscarinic receptors were obtained from the Missouri S&T cDNA Resource Center (Rolla, MO). Cells were cultured in HAM's F12 medium supplemented with fetal calf serum (Biochrom, Berlin, Germany) (10%) and G418 (Biochrom) (750 µg/mL). CHO-hM_2 cell homogenates were prepared according to a reported procedure with minor modifications.[53] The harvest buffer (50 mM TRIS, 1 mM EDTA) was supplemented with

protease inhibitor (SIGMAFAST, Sigma-Aldrich)). Aliquots of 200 µL were transferred to 2-mL cups and stored at −80°C.

Radioligand binding experiments. All radioligand binding experiments were performed at 23 ± 1 °C. Leibovitz L-15 medium (Gibco, Life Technologies GmbH, Darmstadt, Germany) supplemented with 1% BSA (Serva, Heidelberg, Germany) (in the following referred to as L15 medium) was used as binding buffer throughout. The effects of various MR ligands on the equilibrium binding of [^{3}H]NMS (equilibrium competition binding assay) and the effect of **19** on saturation binding of [^{3}H]NMS were determined at intact adherent CHO-hM_xR cells (equilibrium competition binding: x = 1-5, saturation binding: x = 2) in white 96-well plates with clear bottom (Corning Life Sciences, Tewksbury, MA; Corning cat. no. 3610) using the protocol of previously described MR binding studies with [^{3}H]NMS.[32] The concentration of [^{3}H]NMS was 0.2 nM (M_1, M_2, M_3), 0.1 nM (M_4) or 0.3 nM (M_5) and the incubation time was 3 h throughout. For studying the effect of **8** on the M_2R equilibrium binding of [^{3}H]NMS, the radioligand was additionally applied at concentrations of 0.1 and 2 nM. Unspecific binding was determined in the presence of **2** (500-fold excess to [^{3}H]NMS).

Saturation and competition binding experiments as well as association and dissociation experiments with [^{3}H]**19** were performed at intact adherent CHO-hM_2 cells in white 96-well plates with clear bottom (Corning Life Sciences) using the recently described experimental procedure for saturation and equilibrium competition binding studies with [^{3}H]NMS at CHO-hM_xR cells (x = 1-5).[32] In case of competition binding studies the concentration of [^{3}H]**19** was 2 nM. For competition binding experiments with **8** additional concentrations of [^{3}H]**19** were applied (4, 8, 15 and 30 nM). For both, saturation and competition binding studies, the incubation time was 2 h. Unspecific binding was determined in the presence of **2** (500-fold excess to [^{3}H]**19**). For M_2R association experiments with [^{3}H]**19** CHO-hM_2 cells were incubated with [^{3}H]**19** (2 nM) and the incubation was stopped after different periods of time

(between 1 and 140 min) by suction of the radioligand solution, washing of the cells twice with ice-old PBS and further processing as described previously.[32] Unspecific binding was determined in the presence of **2** (400 nM). In case of dissociation experiments cells were preincubated with [^{3}H]**19** (2 nM) for 105 min. The radioligand solution was removed by suction, the cells were covered with L15 medium (200 µL) containing **2** (400 nM), **2** and **8** (400 nM and 100 µM, respectively) or **8** (100 µM), and the plates were gently shaken. After different periods of time (between 0 and 300 min) the cells were washed twice with ice-cold PBS followed by cell lysis and further processing as reported previously.[32] To determine unspecific binding the same procedure was applied, but **2** (400 nM) was added during the preincubation step.

Saturation binding experiments with [^{3}H]**33** and [^{3}H]**47** at live adherent CHO-hM_2 cells (incubation time: 2 h) were performed using white 96-well plates with clear bottom (Corning Life Sciences) and the experimental protocol as for binding studies with [^{3}H]**19** (see above). M_2R association and dissociation experiments with [^{3}H]**33** were performed at intact adherent CHO-hM_2 cells in Primaria 24-well plates (Corning Life Sciences) using the procedure as for association and dissociation experiments with [^{3}H]**19** with the following modifications: the total volume of L15 medium per well was 250 instead of 200 µL, and the volume of PBS for washing steps was 500 instead of 200 µL. Cell lysis was performed with 200 µL of lysis solution (instead of 25 µL). For activity measurements the lysis solution was transferred into 6-mL scintillation vials filled with 3 mL of Rotiscint eco plus (Carl Roth), which were kept at least 1 h in the dark prior to the measurement using a LS 6500 liquid scintillation counter (Beckman-Coulter). For association experiments the concentration of [^{3}H]**33** was 1 nM. The incubation was stopped after different periods of time (between 1 and 140 min). Unspecific binding was determined in the presence of **2** (200 nM). For dissociation experiments cells were preincubated with [^{3}H]**33** (1 nM) for 90 min. The dissociation was started by covering of the cells with L15 medium (250 µL) containing **2** (200 nM), **2** and **8** (200 nM and 100 µM,

respectively) or **8** (100 μM), and was followed over a period of 300 min. Unspecific binding was determined by the addition of **2** (200 nM) during the preincubation period.

For saturation binding experiments with [^{3}H]**33** at intact suspended CHO-hM_2 cells the cell suspension was prepared as follows: Cells (80-100% confluency) were scraped off a 175-cm^2 culture flask and centrifuged at 400 *g* for 5 min. The supernatant was discarded and the cells were re-suspended in L15 medium at a density of 200,000 cells/mL. Saturation binding experiments were performed in Primaria 96-well plates (Corning Life Science) using a final volume of 200 μL per well. For the determination of total binding wells were prefilled with L-15 medium (160 μL) and L15 medium (20 μL) containing [^{3}H]**33** 10-fold concentrated. For the determination of unspecific binding (in the presence of **2**, 500-fold excess to [^{3}H]**33**) wells were prefilled with L-15 medium (140 μL), L15 medium (20 μL) containing **2** 10-fold concentrated and L15 medium (20 μL) containing [^{3}H]**33** 10-fold concentrated. To all wells 20 μL of the CHO-hM_2 cell suspension (200,000 cells/mL) were added and the plates were shaken at 23°C for 2 h. The cell mass was collected on GF/C filter mats (0.26 mm; Whatman, Maidstone, UK) (pretreated with 0.3% polyethylenimine) and washed with cold Tris buffer (Tris (91 g/L), $MgCl_2 \times 6\ H_2O$ (25.5 g/L), EDTA (3.76 g/L)) using a Brandel Harvester (Brandel, Gaithersburg, MD). Filter pieces for each well were punched out and transferred into 1450-401 96-well plates (PerkinElmer). Rotiscint eco plus (Carl Roth) (200 μL) was added and the plates sealed with a transparent sealing tape (permanent seal for microplates, PerkinElmer, prod. no. 1450–461), vigorously shaken for at least 3 h, and afterwards kept in the dark for at least 1 h prior to the measurement of radioactivity (dpm) with a MicroBeta2 plate counter (PerkinElmer, Rodgau, Germany).

Saturation and competition binding experiments with [^{3}H]**33** and saturation binding experiments with [^{3}H]**47** at CHO-hM_2 cell homogenates were performed in Primaria 96-well plates (Corning Life Sciences) according to the procedure for saturation binding experiments with [^{3}H]**33** at intact suspended CHO-hM_2 cells (see above) using 10 μL of cell homogenate

instead of 20 µL of cell suspension. The total volume per well was 100 µL instead of 200 µL, i.e., in case of total binding wells were prefilled with L-15 medium (80 µL) followed by the addition of L15 medium (10 µL) containing the radioligand 10-fold concentrated and cell homogenate (10 µL). On the day of the experiment CHO-hM_2 cell homogenates were thawed and re-suspended using a 1-mL syringe (Henke-Sass Wolf, Tuttlingen, Germany) equipped with a needle (0.90 × 40 mm, B. Braun, Melsungen, Germany) followed by centrifugation at 500 *g* at 4°C for 5 min. The supernatant was discarded and the pellets were re-suspended in L15 medium using a 1-mL syringe equipped with a needle (0.45 × 25 mm, B. Braun). The homogenates were stored on ice until use. The total amount of protein per well was between 25 and 30 µg. Unspecific binding was determined in the presence of **2** (500-fold excess to [^{3}H]**33** or [^{3}H]**47**). In case of competition binding studies with various ligands the concentration of [^{3}H]**33** was 0.5 nM. For competition binding experiments with **8** additional concentrations of [^{3}H]**33** were applied (0.4, 1, 2 and 4 nM). For both, saturation ([^{3}H]**33**, [^{3}H]**47**) and competition ([^{3}H]**33**) binding studies, the incubation period was 2 h.

Comparative saturation binding studies with [^{3}H]NMS, [^{3}H]**19** and [^{3}H]**33** at CHO-hM_2 cell homogenates were performed as saturation binding experiments with [^{3}H]**33** at CHO-hM_2 cell homogenates, but using a final volume of 200 µL per well (as in case of saturation binding experiments with [^{3}H]**33** at intact suspended CHO-hM_2 cells). Comparative saturation binding studies with [^{3}H]NMS, [^{3}H]**19** and [^{3}H]**33** at intact adherent CHO-hM_2 cell were performed as saturation binding experiments with [^{3}H]**19**. For comparative saturation binding studies the incubation periods were 3 h in case of [^{3}H]NMS and 2 h in case of [^{3}H]**19** and [^{3}H]**33**.

Dissociation experiments with [^{3}H]**33** at CHO-hM_2 cell homogenates were performed using the experimental procedure as for saturation binding experiments with [^{3}H]**33** at CHO-hM_2 cell homogenates. The final volume per well during the preincubation with [^{3}H]**33** (1 nM, 90 min) was 200 µL. The dissociation was started by the addition of L15 medium (22 µL) containing **2** (5 µM) after different periods of time (between 3 and 300 min; starting with the

longest incubation time) followed by collection of the homogenates on the filter mats using the harvester. To determine unspecific binding, **2** (500 nM) was added during the preincubation step.

Note: To keep the total volume per well at 200 µL in case of saturation binding experiments performed with [^{3}H]**19** and [^{3}H]NMS in the presence of **8**, **9** or **19**, and at 100 µL in case of saturation binding studies performed with [^{3}H]**33** in the presence of **8**, the addition of L15 medium (20 and 10 µL, respectively) containing **8**, **9** or **19 (**10-fold concentrated) was compensated by an equivalent reduction of the volume of L15 medium added to the wells.

IP1 accumulation assay. The measurement of M_2R stimulated activation of the G-protein mediated pathway was performed applying the IP-One HTRF® assay (Cisbio, Codolet, France) according to the manufacturer's protocol. In brief, HEK-293 cells were grown to a confluency of approx. 70% and transiently co-transfected with the cDNAs of the human M_2 receptor (Missouri S&T cDNA Rescourse Center) and the hybrid G-protein $G\alpha_{qi5\text{-}HA}$ ($G\alpha_q$ protein with the last five amino acids at the C-terminus replaced by the corresponding sequence of $G\alpha_i$; gift from the J. David Gladstone Institutes, San Francisco, CA),[23, 54] applying TransIT-293 Mirus transfection reagent (MoBiTec, Goettingen, Germany). After one day, cells were detached from the culture dish with Versene (Life Technologies GmbH, Darmstadt, Germany), seeded into black 384-well plates (10,000 cells/well) (Greiner Bio-One, Frickenhausen, Germany) and maintained for 24 h at 37 °C. After incubation with the test compounds, dissolved in stimulation buffer (final concentration range from 1 pM up to 100 µM), at 37 °C for 1 h the detection reagents were added (IP1-d2 conjugate and Anti-IP1cryptate TB conjugate, each dissolved in lysis buffer), and incubation was continued at rt for 60 min. Time resolved fluorescence resonance energy transfer (HTRF) was determined using a Clariostar plate reader (BMG, Ortenberg, Germany) measuring fluorescence at 620 (± 10) nm and 670 (± 10) nm (excitation at 330 nm). In the agonist mode, each compound (**19**,

33) was tested in duplicate in three individual experiments in comparison to the reference compound carbachol (**3**, eight experiments). Antagonist properties of **2**, **19** and **33** were determined after preincubation of the cells with **2**, **19** or **33** for 30 min, subsequent addition of the MR agonist 3 (at a final concentration of 0.1, 0.3, 1 or 10 μM) and continued incubation at 37°C for 1 h (at least four independent experiments each).

Molecular dynamics simulation. The crystal structure of the inactive hM_2R bound to the antagonist QNB (PDB ID: 3UON)[22] was used as template. Minor modifications were performed using the modelling suite SYBYL-X 2.0 (Tripos Inc., St. Louis, MO): The ICL3 was reconstituted by insertion of eight alanine residues using the loop search module within SYBYL-X 2.0. Coordinates of non-ligand and non-receptor molecules were removed. The protein preparation wizard (Schrödinger LLC, Portland, OR USA) was used to refine the receptor model: The N- and C-terminus were capped by the introduction of an acetyl and a methylamide group, respectively, and amino acid side chains containing hydrogen bond donors and acceptors were optimized for hydrogen bonding. Histidine residues were simulated in the uncharged form as the N^{ε}-H tautomer. Residues other than histidine were simulated in their dominant protonation state at pH 7. Disulphide bonds were maintained between $C96^{3.25}$ and $C176^{ECL2}$ as well as between $C413^{ECL3}$ and $C416^{ECL3}$, and a sodium ion was placed next to $D69^{2.50}$.[55] Ligand (**19**, **33**) geometries were energetically optimized using the LigPrep module (Schrödinger LLC). Tertiary amine groups in **19** and **33** were protonated resulting in a net charge of +1 and +2, respectively.

'Flexible' docking of **19** and **33** to the hM_2R model was performed using the induced fit docking module (Schrödinger LLC). For initial docking, $Y104^{3.33}$, $Y403^{6.51}$ and $Y426^{7.39}$ were temporarily mutated to alanine, and the ligands **19** and **33** were docked within a box of 30 × 30 × 30 Å and a box of 46 × 46 × 46 Å, respectively, around the crystallographic binding pose of QNB. Prior to redocking, performed in the extended precision mode, a second side chain

trimming (mutation of Y104$^{3.33}$, Y403$^{6.51}$ and Y426$^{7.39}$ to alanine) was executed in case of **33**, and, after redocking, a second prime refinement was applied (including a reversion of the alanine mutations). Among the reasonable ligand binding poses, the pose, corresponding to the lowest XP GScore, was selected as template for the MD simulation.

The respective ligand-receptor complexes were aligned to the hM_2R entry (PDB ID: 3UON) in the orientations of proteins in membranes (OPM) database[56] using the protein structure alignment tool (Schrödinger LLC). The CHARMM GUI[57-61] interface was used to insert the prepared ligand-receptor complexes into a hydrated, equilibrated palmitoyloleoylphosphatidylcholine (POPC) bilayer, comprising 180 POPC molecules as well as sodium chloride at a concentration of 150 mM (net charge of the entire system was zero). The system contained about 72,000 (**19**) and 81,000 (**33**) atoms and the box size was approximately 86 × 86 × 106 Å and 86 × 86 × 118 Å, respectively. The CHARMM36 parameter set was used for the protein structure,[62-64] lipid,[65] and inorganic ions,[66] and the CHARMM TIP3P model for water[67] to define the geometry and partial charges. The protein parameters included CMAP terms. Ligand geometry and partial charge parameters were derived from the CHARMM ParamChem web server, version 1.0.0[68-71]. Each simulation was executed on one Nvidia GTX 1080 GPU (approx. 9 TFlops) using the CUDA version of PMEMD,[72, 73] implemented in AMBER16 (AMBER 2016, University of California, San Francisco, CA). After minimization, the system was heated from 0 to 100 K in the NVT ensemble during 50 ps and from 100 to 310 K in the NPT ensemble during 450 ps, applying harmonic restraints of 10 kcal · mol^{-1} · Å^{-1} to protein and ligand atoms as well as 2.5 kcal · mol^{-1} · Å^{-1} to POPC atoms. At the first heating step (0 to 100 K), initial velocities were randomly assigned using Langevin dynamics. The simulation systems were successively equilibrated at 310 K in the NPT ensemble using a Langevin thermostat,[74, 75] a collision frequency of 1.0 ps^{-1} and a Berendsen barostat[76] with semi-isotropic pressure scaling maintaining a target pressure of 1 bar with a pressure relaxation time of 0.5 ps. During the

subsequent 10-ns equilibration period harmonic restraints were reduced step-wise (every 2 ns) to 0 kcal · mol^{-1} · $Å^{-1}$. The interaction cut-off was set to 8.0 Å and long-range electrostatics were computed using the particle mesh Ewald (PME) method.[77] Bonds involving hydrogen atoms were constrained using SHAKE[78] to enable a frame step size of 2 fs. The final frame of the equilibration period was used as input for the simulations over 2 μs (**19**) and 3 μs (**33**). The 'production runs' were essentially performed as the equilibration runs, but the Berendsen barostat was replaced by the Monte Carlo Barostat. Data were collected every 100 ps and analyzed by means of cpptraj every ns. For cluster analysis, the average linkage algorithm[79] was applied, setting a cluster size of 5 (*cf*. Table S1). H-bond plots were prepared with the programming language R (R Development Core Team (2008), R: A language and environment for statistical computing, R Foundation for Statistical Computing, Vienna, Austria, http://www.R-project.org; Karline Soetaert (2016), plot3D: Plotting Multi-Dimensional Data, R package version 1.1, https://CRAN.R-project.org/package=plot3D; Philip Johnson (2015), devEMF: EMF Graphics Output Device, R package version 2.0, https://CRAN.R-project.org/package=devEMF). Figures showing molecular structures of the M_2R in complex with **19** or **33** were generated with PyMOL Molecular Graphics system, version 1.8.2.1 (Schrödinger LLC). The movie was rendered using UCSF Chimera.[80]

Data processing. Retention (capacity) factors were calculated from retention times (t_R) according to $k = (t_R - t_0)/t_0$ (t_0 = dead time). Data of the IP1 accumulation assay (agonist mode) were processed by plotting the ratios (emission 670 nm/emission 620 nm) of the HTRF measurements against log(concentration **3**) and analysis by a four-parameter logistic equation (GraphPad Prism Software 6.0, GraphPad Software, San Diego, CA), followed by normalization (0% = 'top' (maximum of IP1 accumulation), 100% = 'bottom' (basal activity)) and analysis of the normalized data by a four-parameter logistic equation (log(agonist) *vs*. response - variable slope). Data of the IP1 accumulation assay (antagonist mode; inhibition of

the response elicited by 0.1, 0.3, 1 or 10 μM **3**) were processed by plotting the fluorescence ratio against log(concentration antagonist) and analysis by a four-parameter logistic equation (GraphPad Prism), followed by normalization (0% = maximum IP1 accumulation elicited by **3** (obtained from one or two control concentration-response curves on the same plate), 100% = 'bottom' (basal activity)) and analysis of the normalized data by a four-parameter logistic equation (log(inhibitor) vs. response - variable slope). pIC_{50} values were converted into pK_b values according to the Cheng-Prusoff equation[81] (logarithmic form). Specific binding data (dpm) from saturation binding experiments were plotted against the free radioligand concentration and analyzed by a two-parameter equation describing hyperbolic binding (one site-specific binding, GraphPad Prism) to obtain K_d and B_{max} values. In case of low unspecific binding ([^{3}H]**19**, [^{3}H]**33** (cell homogenates and intact CHO-hM_2 cells in suspension)) the free radioligand concentration (nM) was calculated by subtracting the amount of specifically bound radioligand (nM) (calculated from the specifically bound radioligand in dpm, the specific activity and the volume per well) from the total radioligand concentration. In case of high unspecific binding ([^{3}H]**33** (intact adherent CHO-hM_2 cells), [^{3}H]**47** (intact adherent CHO-hM_2 cells and cell homogenates)) the free radioligand concentration (nM) was calculated by subtracting the amount of specifically and unspecifically bound radioligand (nM) from the total radioligand concentration. Unspecific binding data from saturation binding experiments were fitted by linear regression. In case of saturation binding experiments with [^{3}H]**19** and [^{3}H]**33** in the presence of compounds **8** or **9** as well as saturation binding experiments with [^{3}H]NMS in the presence of **19**, specific binding data were normalized to the B_{max} value, and specific binding (%) was plotted against the radioligand concentration as well as against log(radioligand concentration) followed by analysis using a two-parameter equation describing hyperbolic binding (one site-specific binding, GraphPad Prism) and a four-parameter logistic fit (log(agonist) *vs*. response-variable slope, GraphPad Prism), respectively, to obtain K_d and pK_d values, respectively. Data for the

'Schild' analysis were obtained from the rightward shift (ΔpK_d) of the saturation isotherm and transformation into log(r−1) (where $r = 10^{\Delta pKd}$). Log(r−1) was plotted against log(concentration **8**, **9** or **19**) and the data were analyzed by linear regression to obtain the slope and the 'pA_2' values (intercept with the X axis). Specific binding data from association experiments with [^{3}H]**19** and [^{3}H]**33** were analyzed by a two-parameter equation describing an exponential rise to a maximum (one-phase association, GraphPad Prism) to obtain the observed association rate constant k_{obs} and the maximum of specifically bound radioligand ($B_{(eq)}$) which was used to calculate specifically bound radioligand ($B_{(t)}$) in %. Data from dissociation experiments (% specifically bound radioligand ($B_{(t)}$) plotted over time) were analyzed by a three-parameter equation (one phase decay, GraphPad Prism) (in case of [^{3}H]**19** 'plateau' was defined as 0) to obtain the dissociation rate constant k_{off}. The association rate constants (k_{on}) of the radiolabeled dibenzodiazepinone derivatives were calculated from k_{obs}, k_{off} and the radioligand concentration ([RL]) according to the correlation: $k_{on} = (k_{obs}\text{-}k_{off})/[RL]$. Total binding data (dpm) from radioligand competition binding experiments (determination of the effect of various MR ligands on the equilibrium binding of [^{3}H]NMS, [^{3}H]**19** or [^{3}H]**33**) were plotted against log(concentration competitor) and analyzed by a four-parameter logistic equation (log(inhibitor) vs. response-variable slope, GraphPad Prism) followed by normalization (100% = 'top' of the four-parameter logistic fit, 0% = unspecifically bound radioligand (dpm) determined in the presence of **2** at 200 or 500-fold excess) and analysis of the normalized data by a four-parameter logistic equation (effect of **8** on the equilibrium binding of [^{3}H]NMS, [^{3}H]**19** or [^{3}H]**33**; *cf.* Fig. 8) or by a four-parameter logistic equation fused to the Cheng-Prosuff equation (logarithmic form) (equation 1) to obtain pIC_{50} and pK_i values, respectively. Propagated errors were calculated according to the Gaussian law of errors. Statistical significance was assessed by a one-sample *t*-test (curve slopes and lower curve plateaus) or by a One-way ANOVA (no matching or pairing - multiple comparison test using statistical hypothesis testing (Tukey), GraphPad Prism) (K_d values from comparative

saturation binding studies with [^{3}H]NMS, [^{3}H]**19** and [^{3}H]**33**). Equal distribution of the data was assumed.

(equation 1)

$$logIC50 = log(10\text{^}logKi * (1 + HotNM/HotKdNM))$$

$$Y = (Bottom - Top)/(1 + 10\text{^}((X - LogIC50) * HillSlope)) + Top$$

HotNM = radioligand concentration in nM, HotKdNM = Dissociation constant (K_d) of the radioligand in nM

ASSOCIATED CONTENT

Supporting Information. Experimental description of the synthesis and analytical data of compounds **23-29** and **41-45**; Figures S1-S13; Table S1; ^{1}H-NMR and ^{13}C-NMR spectra of compounds **31**, **33**, **46**, **47**, **50** and **52**; RP-HPLC chromatograms of compounds **31**, **33**, **46**, **47**, **50** and **52**.

AUTHOR INFORMATION

Corresponding Author

*E-mail: max.keller@chemie.uni-regensburg.de. Phone: (+49)941-9433329. Fax: (+49)941-9434820

Notes

The authors declare no competing financial interest.

ACKNOWLEDGMENT

The authors thank Brigitte Wenzl, Dita Fritsch, Susanne Bollwein and Maria Beer-Krön for excellent technical assistance, Armin Buschauer for providing laboratory equipment and for helpful suggestions, as well as the Leibnitz Rechenzentrum (LRZ) in Munich for providing

software (Schrödinger Suite) and computing resources. This work was funded by the Graduate Training Program (Graduiertenkolleg) GRK1910 of the Deutsche Forschungsgemeinschaft (DFG).

ABBREVIATIONS

B_{max}, maximum number of binding sites; br s, broad singlet; CH_2Cl_2, dichloromethane; CMAP, (grid-based) correction map; DIPEA, diisopropylethylamine; dpm, disintegrations per minute; EtOAc, ethyl acetate; HBTU, *O*-(1*H*-benzotriazol-1-yl)-*N,N,N′,N′*-tetramethyluronium hexafluorophosphate; H_2NOH, hydroxylamine; HOBt, 1*H*-benzotriazol-1-ol; IP1, inositol monophosphate; k, retention (or capacity) factor (HPLC); K_d, dissociation (or binding) constant obtained from a saturation binding experiment; K_i, dissociation (or binding) constant obtained from a competition binding experiment; MeCN, acetonitrile; MR, muscarinic receptor; M_xR, muscarinic M_x (x = 1-5) receptor; NPT, constant number of particles, pressure and temperature; NVT, constant number of particles, volume and temperature; PBS, phosphate buffered saline; pIC_{50}, negative logarithm of the half-maximum inhibitory concentration in M; pK_d, negative logarithm of the K_d in M; pK_i, negative logarithm of the K_i in M; POPC, palmitoyloleoylphosphatidylcholine; RP-HPLC, reversed-phase HPLC; SEM, standard error of the mean

REFERENCES

(1) Eglen, R. M. Overview of muscarinic receptor subtypes. *Handb. Exp. Pharmacol.* **2012,** *208*, 3-28.

(2) Eglen, R. M.; Choppin, A.; Watson, N. Therapeutic opportunities from muscarinic receptor research. *Trends Pharmacol. Sci.* **2001,** *22*, 409-414.

(3) Sheardown, M. J. Muscarinic M1receptor agonists and M2 receptor antagonists as therapeutic targets in Alzheimer's disease. *Expert Opin. Ther. Pat.* **2002,** *12*, 863-870.

(4) Clader, J. W.; Wang, Y. Muscarinic receptor agonists and antagonists in the treatment of Alzheimer's disease. *Curr. Pharm. Des.* **2005,** *11*, 3353-3361.

(5) Citron, M. Alzheimer's disease: strategies for disease modification. *Nat. Rev. Drug Discovery* **2010,** *9*, 387-398.

(6) Conn, P. J.; Christopoulos, A.; Lindsley, C. W. Allosteric modulators of GPCRs: a novel approach for the treatment of CNS disorders. *Nat Rev Drug Discovery* **2009,** *8*, 41-54.

(7) Kruse, A. C.; Hu, J.; Pan, A. C.; Arlow, D. H.; Rosenbaum, D. M.; Rosemond, E.; Green, H. F.; Liu, T.; Chae, P. S.; Dror, R. O.; Shaw, D. E.; Weis, W. I.; Wess, J.; Kobilka, B. K. Structure and dynamics of the M3 muscarinic acetylcholine receptor. *Nature* **2012,** *482*, 552-556.

(8) Birdsall, N. J. M.; Lazareno, S. Allosterism at muscarinic receptors: ligands and mechanisms. *Mini Rev. Med. Chem.* **2005,** *5*, 523-543.

(9) Conn, P. J.; Jones, C. K.; Lindsley, C. W. Subtype-selective allosteric modulators of muscarinic receptors for the treatment of CNS disorders. *Trends Pharmacol. Sci.* **2009,** *30*, 148-155.

(10) Clark, A. L.; Mitchelson, F. The inhibitory effect of gallamine on muscarinic receptors. *Br. J. Pharmacol.* **1976,** *58*, 323-331.

(11) Luellmann, H.; Ohnesorge, F. K.; Schauwecker, G. C.; Wassermann, O. Inhibition of the actions of carbachol and DFP [disopropyl phosphorofluoridate] on guinea pig isolated atria by alkane-bis-ammonium compounds. *Eur. J. Pharmacol.* **1969,** *6*, 241-247.

(12) Croy, C. H.; Schober, D. A.; Xiao, H.; Quets, A.; Christopoulos, A.; Felder, C. C. Characterization of the novel positive allosteric modulator, LY2119620, at the muscarinic M2 and M4 receptors. *Mol. Pharmacol.* **2014,** *86*, 106-115.

(13) Schober, D. A.; Croy, C. H.; Xiao, H.; Christopoulos, A.; Felder, C. C. Development of a radioligand, [(3)H]LY2119620, to probe the human M(2) and M(4) muscarinic receptor allosteric binding sites. *Mol. Pharmacol.* **2014,** *86*, 116-123.

(14) Kruse, A. C.; Kobilka, B. K.; Gautam, D.; Sexton, P. M.; Christopoulos, A.; Wess, J. Muscarinic acetylcholine receptors: novel opportunities for drug development. *Nat. Rev. Drug Discovery* **2014,** *13*, 549-560.

(15) Trankle, C.; Weyand, O.; Voigtlander, U.; Mynett, A.; Lazareno, S.; Birdsall Nigel, J. M.; Mohr, K. Interactions of orthosteric and allosteric ligands with [3H]dimethyl-W84 at the common allosteric site of muscarinic M2 receptors. *Mol. Pharmacol.* **2003,** *64*, 180-190.

(16) Christopoulos, A.; Changeux, J. P.; Catterall, W. A.; Fabbro, D.; Burris, T. P.; Cidlowski, J. A.; Olsen, R. W.; Peters, J. A.; Neubig, R. R.; Pin, J. P.; Sexton, P. M.; Kenakin, T. P.; Ehlert, F. J.; Spedding, M.; Langmead, C. J. International Union of Basic and Clinical Pharmacology. XC. multisite pharmacology: recommendations for the nomenclature of receptor allosterism and allosteric ligands. *Pharmacol. Rev.* **2014,** *66*, 918-947.

(17) Antony, J.; Kellershohn, K.; Mohr-Andrae, M.; Kebig, A.; Prilla, S.; Muth, M.; Heller, E.; Disingrini, T.; Dallanoce, C.; Bertoni, S.; Schrobang, J.; Traenkle, C.; Kostenis, E.; Christopoulos, A.; Hoeltje, H.-D.; Barocelli, E.; De Amici, M.; Holzgrabe, U.; Mohr, K. Dualsteric GPCR targeting: a novel route to binding and signaling pathway selectivity. *FASEB J.* **2009,** *23*, 442-450.

(18) De Amici, M.; Dallanoce, C.; Holzgrabe, U.; Trankle, C.; Mohr, K. Allosteric ligands for G protein-coupled receptors: a novel strategy with attractive therapeutic opportunities. *Med. Res. Rev.* **2010,** *30*, 463-549.

(19) Valant, C.; Lane, J. R.; Sexton, P. M.; Christopoulos, A. The best of both worlds? Bitopic orthosteric/allosteric ligands of G protein-coupled receptors. *Annu. Rev. Pharmacol. Toxicol.* **2012,** *52*, 153-178.

(20) Lane, J. R.; Sexton, P. M.; Christopoulos, A. Bridging the gap: bitopic ligands of G-protein-coupled receptors. *Trends Pharmacol. Sci.* **2013,** *34*, 59-66.

(21) Christopoulos, A. Advances in G protein-coupled receptor allostery: from function to structure. *Mol. Pharmacol.* **2014,** *86*, 463-478.

(22) Haga, K.; Kruse, A. C.; Asada, H.; Yurugi-Kobayashi, T.; Shiroishi, M.; Zhang, C.; Weis, W. I.; Okada, T.; Kobilka, B. K.; Haga, T.; Kobayashi, T. Structure of the human M2 muscarinic acetylcholine receptor bound to an antagonist. *Nature* **2012,** *482*, 547-551.

(23) Kruse, A. C.; Ring, A. M.; Manglik, A.; Hu, J.; Hu, K.; Eitel, K.; Hubner, H.; Pardon, E.; Valant, C.; Sexton, P. M.; Christopoulos, A.; Felder, C. C.; Gmeiner, P.; Steyaert, J.; Weis, W. I.; Garcia, K. C.; Wess, J.; Kobilka, B. K. Activation and allosteric modulation of a muscarinic acetylcholine receptor. *Nature* **2013,** *504*, 101-106.

(24) Thal, D. M.; Sun, B.; Feng, D.; Nawaratne, V.; Leach, K.; Felder, C. C.; Bures, M. G.; Evans, D. A.; Weis, W. I.; Bachhawat, P.; Kobilka, T. S.; Sexton, P. M.; Kobilka, B. K.; Christopoulos, A. Crystal structures of the M1 and M4 muscarinic acetylcholine receptors. *Nature* **2016,** *531*, 335-340.

(25) Mohr, M.; Heller, E.; Ataie, A.; Mohr, K.; Holzgrabe, U. Development of a new type of allosteric modulator of muscarinic receptors: hybrids of the antagonist AF-DX 384 and the hexamethonio derivative W84. *J. Med. Chem.* **2004,** *47*, 3324-3327.

(26) Disingrini, T.; Muth, M.; Dallanoce, C.; Barocelli, E.; Bertoni, S.; Kellershohn, K.; Mohr, K.; De Amici, M.; Holzgrabe, U. Design, synthesis, and action of oxotremorine-related hybrid-type allosteric modulators of muscarinic acetylcholine receptors. *J. Med. Chem.* **2006,** *49*, 366-372.

(27) Steinfeld, T.; Mammen, M.; Smith, J. A.; Wilson, R. D.; Jasper, J. R. A novel multivalent ligand that bridges the allosteric and orthosteric binding sites of the M2 muscarinic receptor. *Mol. Pharmacol.* **2007,** *72*, 291-302.

(28) Bock, A.; Mohr, K. Dualsteric GPCR targeting and functional selectivity: the paradigmatic M(2) muscarinic acetylcholine receptor. *Drug Discovery Today: Technol.* **2013,** *10*, e245-252.

(29) Schmitz, J.; van der Mey, D.; Bermudez, M.; Klockner, J.; Schrage, R.; Kostenis, E.; Trankle, C.; Wolber, G.; Mohr, K.; Holzgrabe, U. Dualsteric muscarinic antagonists--orthosteric binding pose controls allosteric subtype selectivity. *J. Med. Chem.* **2014,** *57*, 6739-6750.

(30) Trankle, C.; Andresen, I.; Lambrecht, G.; Mohr, K. M2 receptor binding of the selective antagonist AF-DX 384: possible involvement of the common allosteric site. *Mol. Pharmacol.* **1998,** *53*, 304-312.

(31) Mitchelson, F. J. The pharmacology of McN-A-343. *Pharmacol. Ther.* **2012,** *135*, 216-245.

(32) Keller, M.; Trankle, C.; She, X.; Pegoli, A.; Bernhardt, G.; Buschauer, A.; Read, R. W. M2 Subtype preferring dibenzodiazepinone-type muscarinic receptor ligands: Effect of chemical homo-dimerization on orthosteric (and allosteric?) binding. *Bioorg. Med. Chem.* **2015,** *23*, 3970-3990.

(33) Eberlein, W. G.; Engel, W.; Mihm, G.; Rudolf, K.; Wetzel, B.; Entzeroth, M.; Mayer, N.; Doods, H. N. Structure-activity relationships and pharmacological profile of selective tricyclic antimuscarinics. *Trends Pharmacol. Sci.* **1989,** *Suppl*, 50-54.

(34) Dimick, S. M.; Powell, S. C.; McMahon, S. A.; Moothoo, D. N.; Naismith, J. H.; Toone, E. J. On the meaning of affinity: cluster glycoside effects and concanavalin A. *J. Am. Chem. Soc.* **1999,** *121*, 10286-10296.

(35) Park, J.; Wang, Z. U.; Sun, L.-B.; Chen, Y.-P.; Zhou, H.-C. Introduction of functionalized mesopores to metal–organic frameworks via metal–ligand–fragment coassembly. *J. Am. Chem. Soc.* **2012,** *134*, 20110-20116.

(36) Bailey, P. D.; Beard, M. A.; Dang, H. P. T.; Phillips, T. R.; Price, R. A.; Whittaker, J. H. Debenzylation using catalytic hydrogenolysis in trifluoroethanol, and the total synthesis of (-)-raumacline. *Tetrahedron Lett.* **2008,** *49*, 2150-2153.

(37) Copeland, R. A. Conformational adaptation in drug-target interactions and residence time. *Future Med. Chem.* **2011,** *3*, 1491-1501.

(38) Vauquelin, G. Simplified models for heterobivalent ligand binding: when are they applicable and which are the factors that affect their target residence time. *Naunyn-Schmiedeberg's Arch. Pharmacol.* **2013,** *386*, 949-962.

(39) Hulme, E. C.; Trevethick, M. A. Ligand binding assays at equilibrium: validation and interpretation. *Br. J. Pharmacol.* **2010,** *161*, 1219-1237.

(40) Christopoulos, A.; Kenakin, T. G protein-coupled receptor allosterism and complexing. *Pharmacol. Rev.* **2002,** *54*, 323-374.

(41) Dei, S.; Bellucci, C.; Buccioni, M.; Ferraroni, M.; Guandalini, L.; Manetti, D.; Martini, E.; Marucci, G.; Matucci, R.; Nesi, M.; Romanelli, M. N.; Scapecchi, S.; Teodori, E. Synthesis, affinity profile, and functional activity of muscarinic antagonists with a 1-methyl-2-(2,2-alkylaryl-1,3-oxathiolan-5-yl)pyrrolidine structure. *J. Med. Chem.* **2007,** *50*, 1409-1413.

(42) Jakubik, J.; El-Fakahany, E. E.; Dolezal, V. Differences in kinetics of xanomeline binding and selectivity of activation of G proteins at M(1) and M(2) muscarinic acetylcholine receptors. *Mol. Pharmacol.* **2006,** *70*, 656-666.

(43) Kenakin, T. P. *A Pharmacology Primer: Theory, Applications, and Methods*. 3rd ed.; Elsevier Academic Press: Burlington, 2009.

(44) Hedlund, P. B.; Carson, M. J.; Sutcliffe, J. G.; Thomas, E. A. Allosteric regulation by oleamide of the binding properties of 5-hydroxytryptamine7 receptors. *Biochem. Pharmacol.* **1999,** *58*, 1807-1813.

(45) Gregory Karen, J.; Sexton Patrick, M.; Christopoulos, A. Overview of receptor allosterism. *Curr. Protoc. Pharmacol.* **2010,** *Chapter 1*, Unit 1 21.

(46) Suga, H.; Ehlert, F. J. Effects of asparagine mutagenesis of conserved aspartic acids in helix 2 (D2.50) and 3 (D3.32) of M1-M4 muscarinic receptors on the irreversible binding of nitrogen mustard analogs of acetylcholine and McN-A-343. *Biochemistry* **2013,** *52*, 4914-4928.

(47) Keller, M.; Maschauer, S.; Brennauer, A.; Tripal, P.; Koglin, N.; Dittrich, R.; Bernhardt, G.; Kuwert, T.; Wester, H. J.; Buschauer, A.; Prante, O. Prototypic ^{18}F-labeled argininamide-type neuropeptide Y Y_1R antagonists as tracers for PET imaging of mammary carcinoma. *ACS Med. Chem. Lett.* **2017,** *8*, 304-309.

(48) Cohen, V. I.; Baumgold, J.; Jin, B.; De La Cruz, R.; Rzeszotarski, W. J.; Reba, R. C. Synthesis and structure-activity relationship of some 5-[[[(dialkylamino)alkyl]-1-piperidinyl]acetyl]-10,11-dihydro-5H- benzo[b,e][1,4]diazepin-11-ones as M2-selective antimuscarinics. *J. Med. Chem.* **1993,** *36*, 162-165.

(49) Kane, B. E.; Grant, M. K. O.; El-Fakahany, E. E.; Ferguson, D. M. Synthesis and evaluation of xanomeline analogs—Probing the wash-resistant phenomenon at the M1 muscarinic acetylcholine receptor. *Bioorg. Med. Chem.* **2008,** *16*, 1376-1392.

(50) Galli, U.; Ercolano, E.; Carraro, L.; Roman, C. R. B.; Sorba, G.; Canonico, P. L.; Genazzani, A. A.; Tron, G. C.; Billington, R. A. Synthesis and biological evaluation of isosteric analogues of FK866, an inhibitor of NAD salvage. *ChemMedChem* **2008,** *3*, 771-779.

(51) Ruger, C.; Rohnert, H.; Lohmann, D. [New derivatives of 5,10-dihydro-11H-dibenzo[b,e][1,4]diazepine-11-ones with anticholinergic activity]. *Pharmazie* **1990,** *45*, 555-559.

(52) Keller, M.; Kuhn, K. K.; Einsiedel, J.; Hubner, H.; Biselli, S.; Mollereau, C.; Wifling, D.; Svobodova, J.; Bernhardt, G.; Cabrele, C.; Vanderheyden, P. M.; Gmeiner, P.; Buschauer, A. Mimicking of arginine by functionalized N(omega)-carbamoylated arginine as a new broadly applicable approach to labeled bioactive peptides: high affinity angiotensin, neuropeptide Y, neuropeptide FF, and neurotensin receptor ligands as examples. *J. Med. Chem.* **2016,** *59*, 1925-1945.

(53) Hübner, H.; Haubmann, C.; Utz, W.; Gmeiner, P. Conjugated enynes as nonaromatic catechol bioisosteres: synthesis, binding experiments, and computational studies of novel dopamine receptor agonists recognizing preferentially the D3 subtype. *J. Med. Chem.* **2000,** *43*, 756-762.

(54) Conklin, B. R.; Farfel, Z.; Lustig, K. D.; Julius, D.; Bourne, H. R. Substitution of three amino acids switches receptor specificity of Gq alpha to that of Gi alpha. *Nature* **1993,** *363*, 274-276.

(55) Huang, W.; Manglik, A.; Venkatakrishnan, A. J.; Laeremans, T.; Feinberg, E. N.; Sanborn, A. L.; Kato, H. E.; Livingston, K. E.; Thorsen, T. S.; Kling, R. C.; Granier, S.; Gmeiner, P.; Husbands, S. M.; Traynor, J. R.; Weis, W. I.; Steyaert, J.; Dror, R. O.; Kobilka, B. K. Structural insights into micro-opioid receptor activation. *Nature* **2015,** *524*, 315-321.

(56) Lomize, M. A.; Lomize, A. L.; Pogozheva, I. D.; Mosberg, H. I. OPM: orientations of proteins in membranes database. *Bioinformatics* **2006,** *22*, 623-625.

(57) Jo, S.; Kim, T.; Im, W. Automated builder and database of protein/membrane complexes for molecular dynamics simulations. *PLoS One* **2007,** *2*, e880.

(58) Jo, S.; Kim, T.; Iyer, V. G.; Im, W. CHARMM-GUI: a web-based graphical user interface for CHARMM. *J. Comput. Chem.* **2008,** *29*, 1859-1865.

(59) Brooks, B. R.; Brooks, C. L., 3rd; Mackerell, A. D., Jr.; Nilsson, L.; Petrella, R. J.; Roux, B.; Won, Y.; Archontis, G.; Bartels, C.; Boresch, S.; Caflisch, A.; Caves, L.; Cui, Q.; Dinner, A. R.; Feig, M.; Fischer, S.; Gao, J.; Hodoscek, M.; Im, W.; Kuczera, K.; Lazaridis, T.; Ma, J.; Ovchinnikov, V.; Paci, E.; Pastor, R. W.; Post, C. B.; Pu, J. Z.; Schaefer, M.; Tidor, B.; Venable, R. M.; Woodcock, H. L.; Wu, X.; Yang, W.; York, D. M.; Karplus, M. CHARMM: the biomolecular simulation program. *J. Comput. Chem.* **2009,** *30*, 1545-1614.

(60) Wu, E. L.; Cheng, X.; Jo, S.; Rui, H.; Song, K. C.; Davila-Contreras, E. M.; Qi, Y.; Lee, J.; Monje-Galvan, V.; Venable, R. M.; Klauda, J. B.; Im, W. CHARMM-GUI Membrane Builder toward realistic biological membrane simulations. *J. Comput. Chem.* **2014,** *35*, 1997-2004.

(61) Lee, J.; Cheng, X.; Swails, J. M.; Yeom, M. S.; Eastman, P. K.; Lemkul, J. A.; Wei, S.; Buckner, J.; Jeong, J. C.; Qi, Y.; Jo, S.; Pande, V. S.; Case, D. A.; Brooks, C. L., 3rd; MacKerell, A. D., Jr.; Klauda, J. B.; Im, W. CHARMM-GUI input generator for NAMD, GROMACS, AMBER, OpenMM, and CHARMM/OpenMM simulations using the CHARMM36 additive force field. *J. Chem. Theory Comput.* **2016,** *12*, 405-413.

(62) MacKerell, A. D.; Bashford, D.; Bellott, M.; Dunbrack, R. L.; Evanseck, J. D.; Field, M. J.; Fischer, S.; Gao, J.; Guo, H.; Ha, S.; Joseph-McCarthy, D.; Kuchnir, L.; Kuczera, K.; Lau, F. T.; Mattos, C.; Michnick, S.; Ngo, T.; Nguyen, D. T.; Prodhom, B.; Reiher, W. E.; Roux, B.; Schlenkrich, M.; Smith, J. C.; Stote, R.; Straub, J.; Watanabe, M.; Wiorkiewicz-Kuczera, J.; Yin, D.; Karplus, M. All-atom empirical potential for molecular modeling and dynamics studies of proteins. *J Phys Chem B* **1998,** *102*, 3586-3616.

(63) Mackerell, A. D., Jr.; Feig, M.; Brooks, C. L., 3rd. Extending the treatment of backbone energetics in protein force fields: limitations of gas-phase quantum mechanics in reproducing protein conformational distributions in molecular dynamics simulations. *J. Comput. Chem.* **2004,** *25*, 1400-1415.

(64) Best, R. B.; Zhu, X.; Shim, J.; Lopes, P. E.; Mittal, J.; Feig, M.; Mackerell, A. D., Jr. Optimization of the additive CHARMM all-atom protein force field targeting improved sampling of the backbone phi, psi and side-chain chi(1) and chi(2) dihedral angles. *J. Chem. Theory Comput.* **2012,** *8*, 3257-3273.

(65) Klauda, J. B.; Venable, R. M.; Freites, J. A.; O'Connor, J. W.; Tobias, D. J.; Mondragon-Ramirez, C.; Vorobyov, I.; MacKerell, A. D., Jr.; Pastor, R. W. Update of the CHARMM all-atom additive force field for lipids: validation on six lipid types. *J. Phys. Chem. B* **2010,** *114*, 7830-7843.

(66) Beglov, D.; Roux, B. Finite representation of an infinite bulk system: Solvent boundary potential for computer simulations. *J. Chem. Phys.* **1994,** *100*, 9050-9063.

(67) Jorgensen, W. L.; Chandrasekhar, J.; Madura, J. D.; Impey, R. W.; Klein, M. L. Comparison of simple potential functions for simulating liquid water. *J. Chem. Phys.* **1983,** *79*, 926-935.

(68) Vanommeslaeghe, K.; Hatcher, E.; Acharya, C.; Kundu, S.; Zhong, S.; Shim, J.; Darian, E.; Guvench, O.; Lopes, P.; Vorobyov, I.; Mackerell, A. D., Jr. CHARMM general force field: A force field for drug-like molecules compatible with the CHARMM all-atom additive biological force fields. *J. Comput. Chem.* **2010,** *31*, 671-690.

(69) Vanommeslaeghe, K.; MacKerell, A. D., Jr. Automation of the CHARMM General Force Field (CGenFF) I: bond perception and atom typing. *J. Chem. Inf. Model.* **2012,** *52*, 3144-3154.

(70) Vanommeslaeghe, K.; Raman, E. P.; MacKerell, A. D., Jr. Automation of the CHARMM General Force Field (CGenFF) II: assignment of bonded parameters and partial atomic charges. *J. Chem. Inf. Model.* **2012,** *52*, 3155-3168.

(71) Yu, W.; He, X.; Vanommeslaeghe, K.; MacKerell, A. D., Jr. Extension of the CHARMM General Force Field to sulfonyl-containing compounds and its utility in biomolecular simulations. *J. Comput. Chem.* **2012,** *33*, 2451-2468.

(72) Salomon-Ferrer, R.; Gotz, A. W.; Poole, D.; Le Grand, S.; Walker, R. C. Routine microsecond molecular dynamics simulations with AMBER on GPUs. 2. explicit solvent particle mesh ewald. *J. Chem. Theory Comput.* **2013,** *9*, 3878-3888.

(73) Le Grand, S.; Götz, A. W.; Walker, R. C. SPFP: Speed without compromise—A mixed precision model for GPU accelerated molecular dynamics simulations. *Comput. Phys. Commun.* **2013,** *184*, 374-380.

(74) Uberuaga, B. P.; Anghel, M.; Voter, A. F. Synchronization of trajectories in canonical molecular-dynamics simulations: observation, explanation, and exploitation. *J. Chem. Phys.* **2004,** *120*, 6363-6374.

(75) Sindhikara, D. J.; Kim, S.; Voter, A. F.; Roitberg, A. E. Bad seeds sprout perilous dynamics: stochastic thermostat induced trajectory synchronization in biomolecules. *J. Chem. Theory Comput.* **2009,** *5*, 1624-1631.

(76) Berendsen, H. J. C.; Postma, J. P. M.; van Gunsteren, W. F.; DiNola, A.; Haak, J. R. Molecular dynamics with coupling to an external bath. *J. Chem. Phys.* **1984,** *81*, 3684-3690.

(77) Darden, T.; York, D.; Pedersen, L. Particle mesh Ewald: An N·log(N) method for Ewald sums in large systems. *J. Chem. Phys.* **1993,** *98*, 10089-10092.

(78) Ryckaert, J.-P.; Ciccotti, G.; Berendsen, H. J. C. Numerical integration of the cartesian equations of motion of a system with constraints: molecular dynamics of n-alkanes. *J. Comput. Phys.* **1977,** *23*, 327-341.

(79) Sokal, R. R.; Michener, C. D. A statistical method for evaluating systematic relationships. *Univ. Kansas Sci. Bull.* **1958,** *28*, 1409-1438.

(80) Pettersen, E. F.; Goddard, T. D.; Huang, C. C.; Couch, G. S.; Greenblatt, D. M.; Meng, E. C.; Ferrin, T. E. UCSF Chimera-A visualization system for exploratory research and analysis. *J. Comput. Chem.* **2004,** *25*, 1605-1612.

(81) Cheng, Y.-C.; Prusoff, W. H. Relation between the inhibition constant K1) and the concentration of inhibitor which causes fifty per cent inhibition (I50) of an enzymic reaction. *Biochem. Pharmacol.* **1973,** *22*, 3099-3108.

TOC graphic

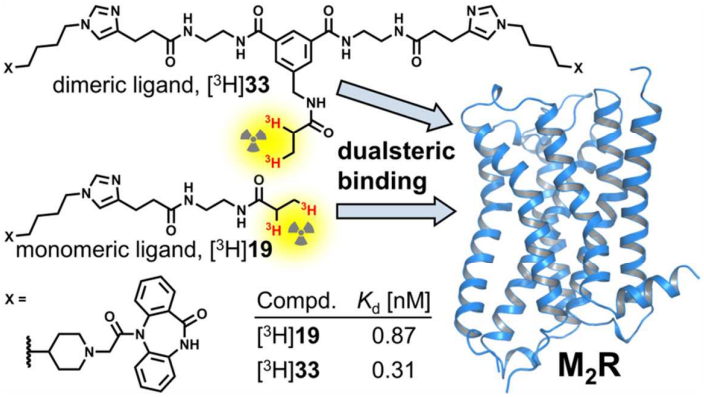
dimeric ligand, [3H]33
dualsteric binding
monomeric ligand, [3H]19
x =
Compd. Kd [nM]
[3H]19 0.87
[3H]33 0.31
M2R

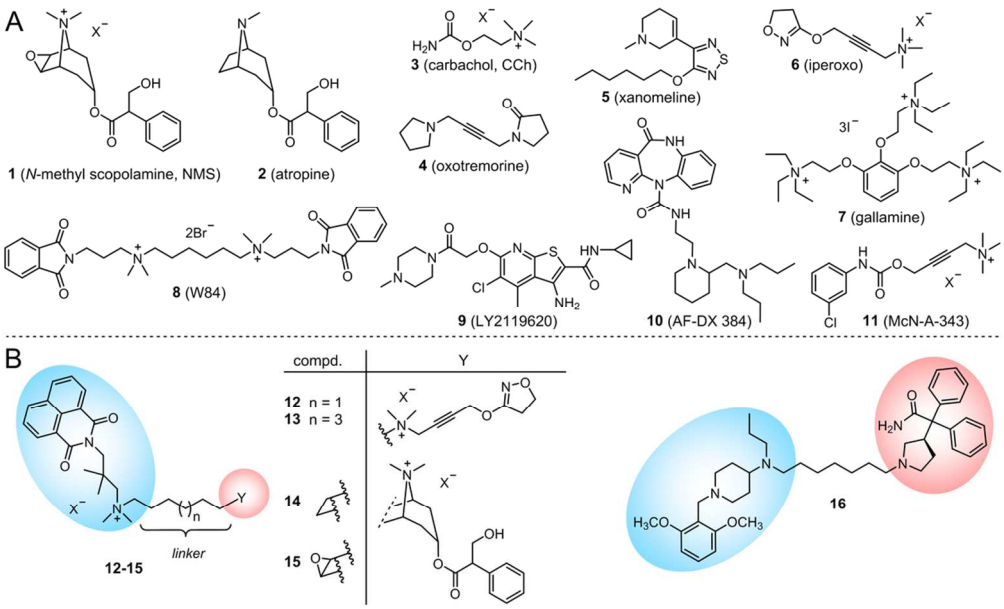

Figure 1

106x63mm (300 x 300 DPI)

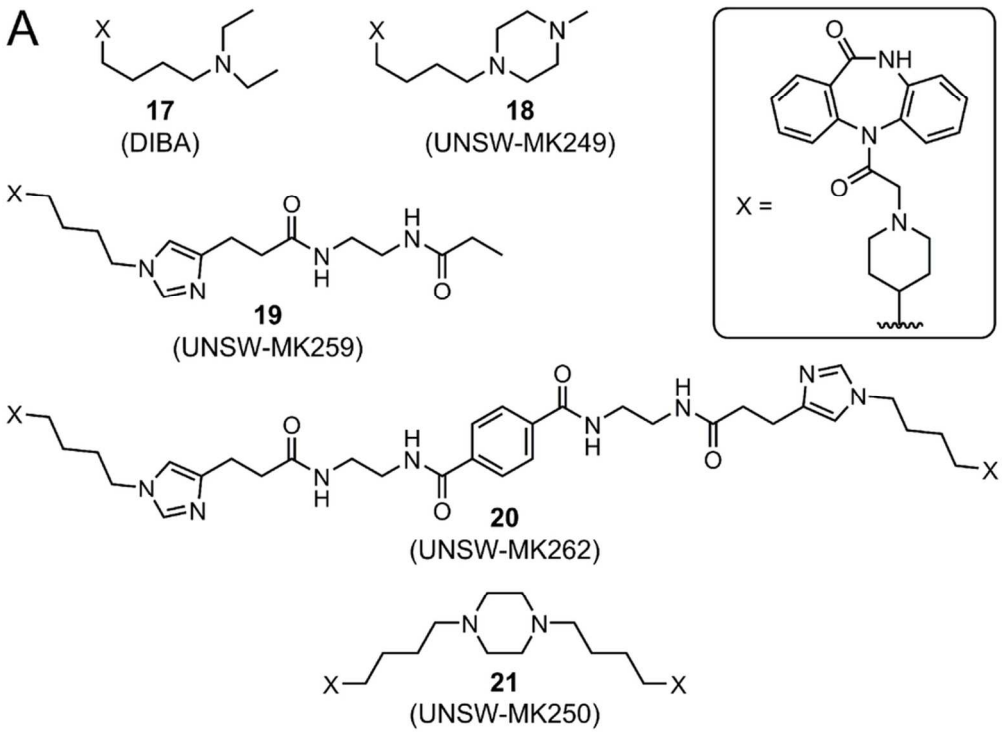

Figure 2

84x84mm (300 x 300 DPI)

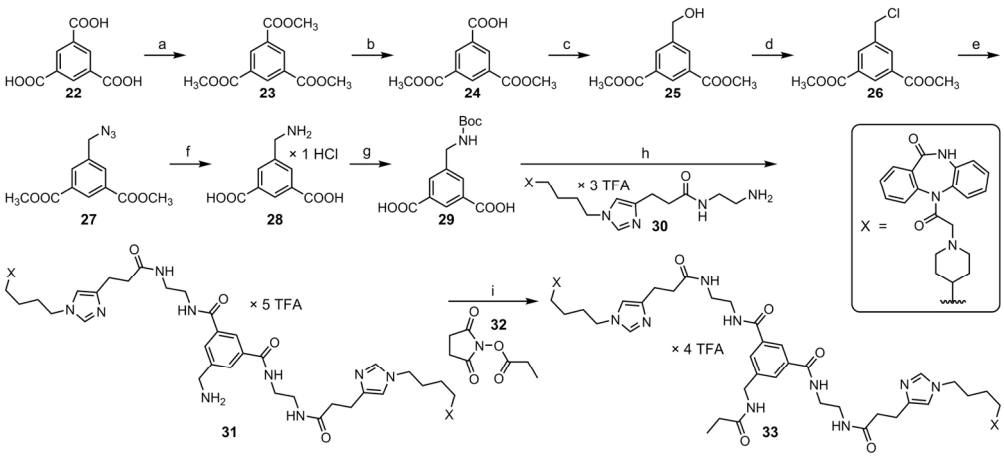

Scheme 1

79x36mm (600 x 600 DPI)

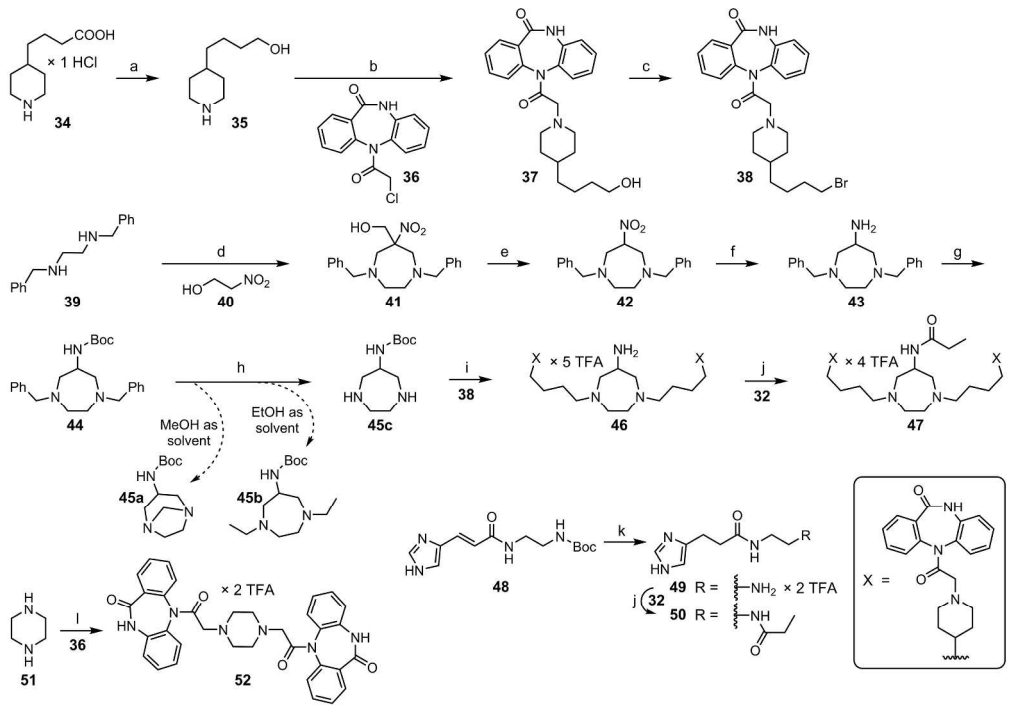

Scheme 2

122x86mm (600 x 600 DPI)

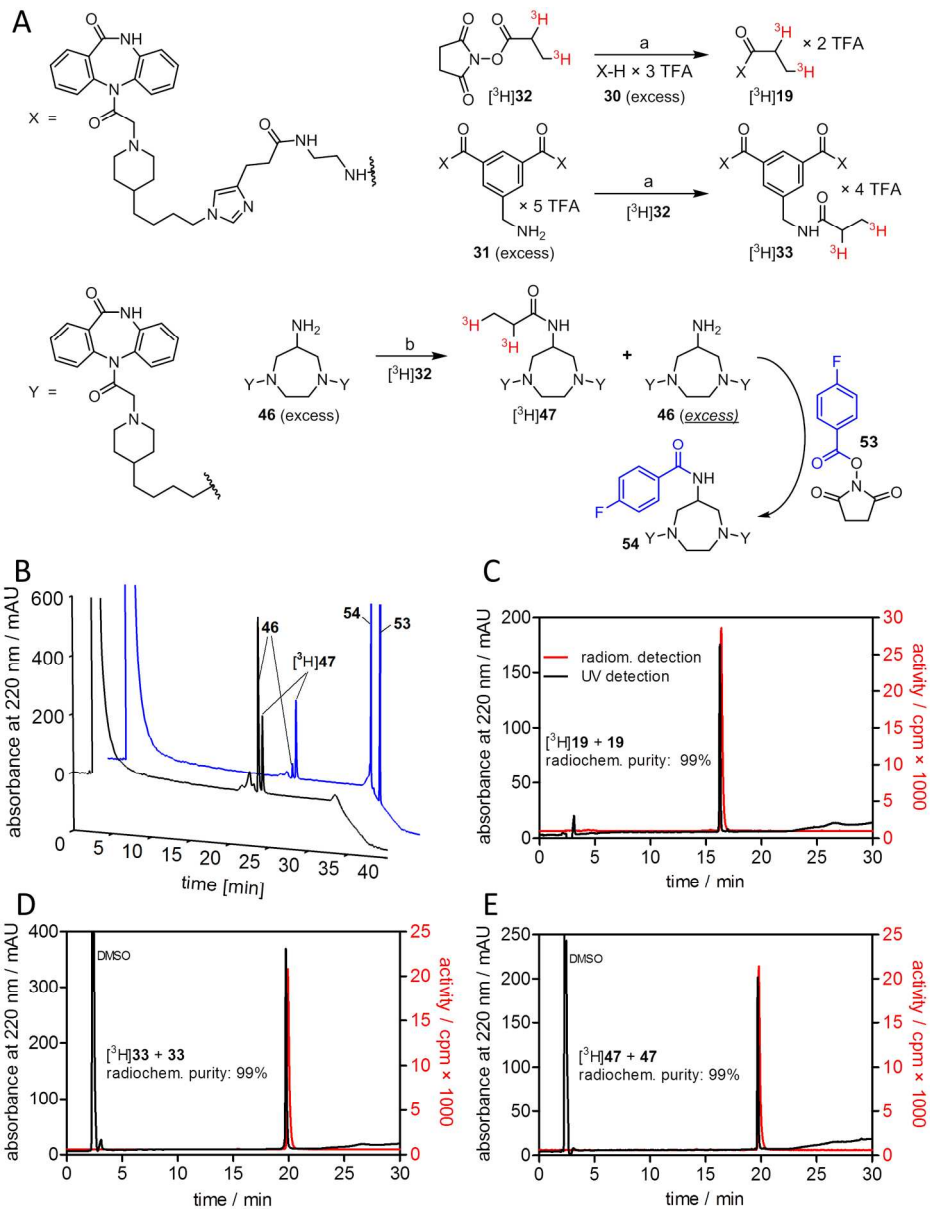

Figure 3

225x291mm (300 x 300 DPI)

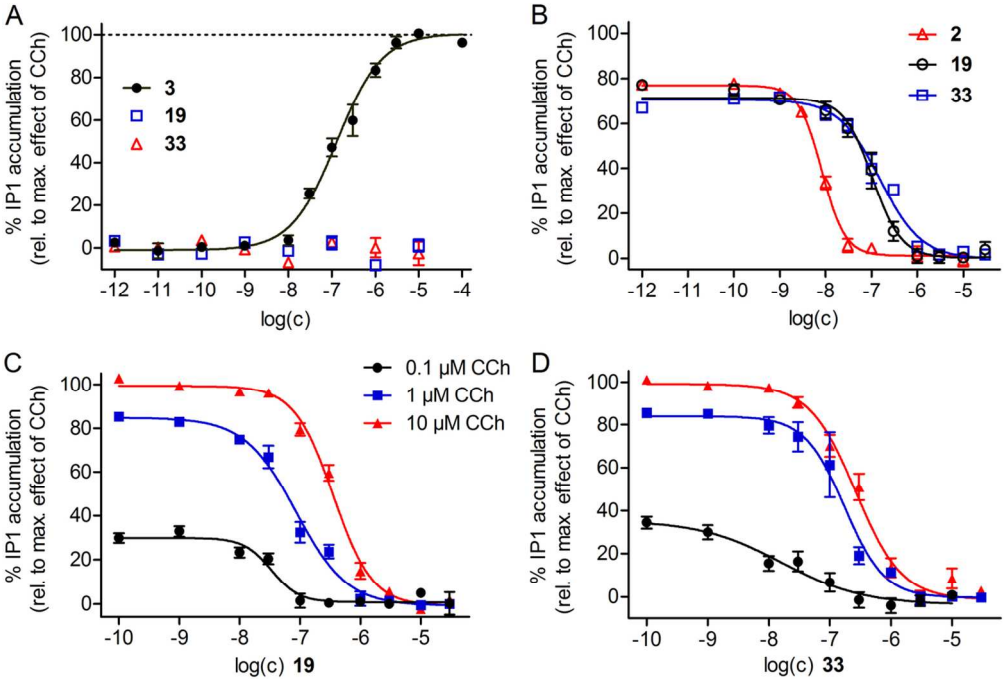

Figure 4

119x80mm (300 x 300 DPI)

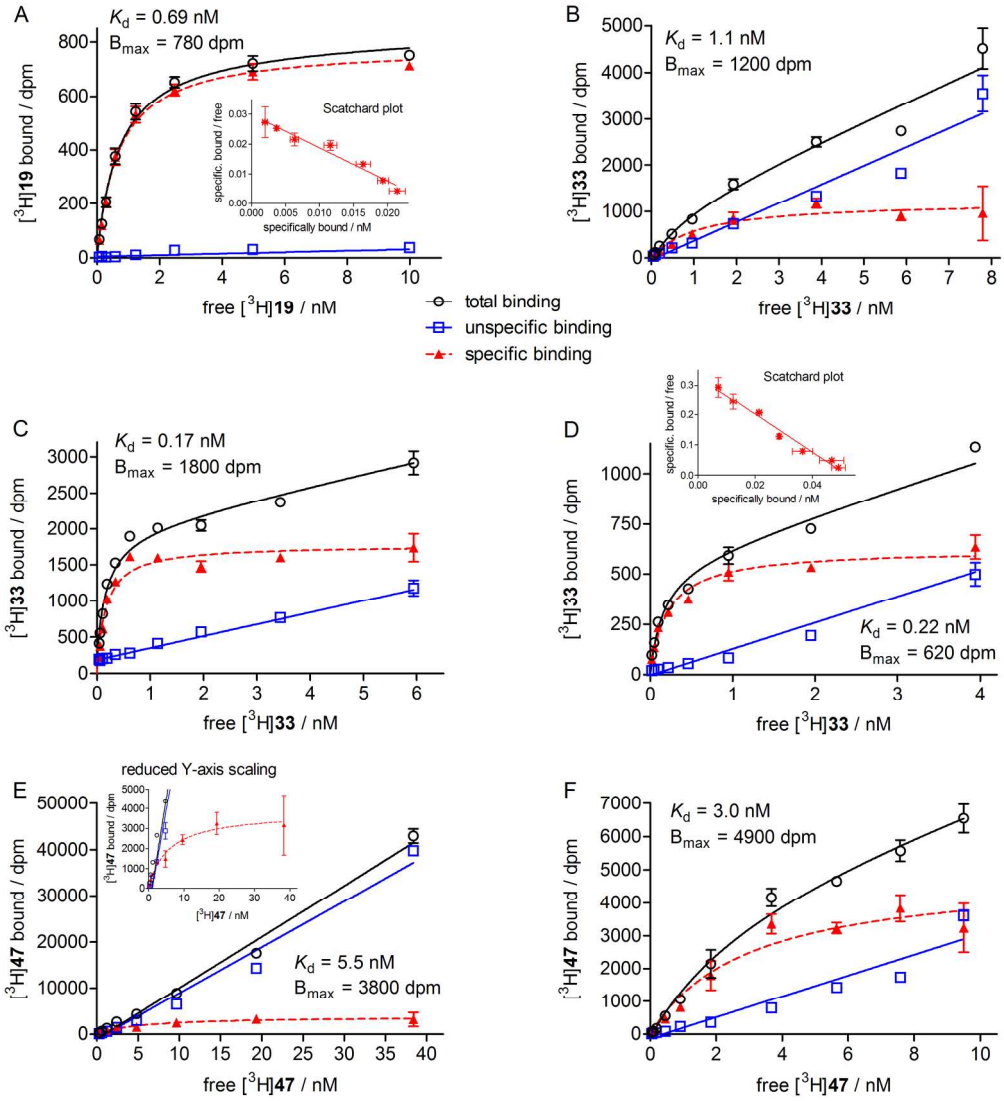

Figure 5

193x212mm (300 x 300 DPI)

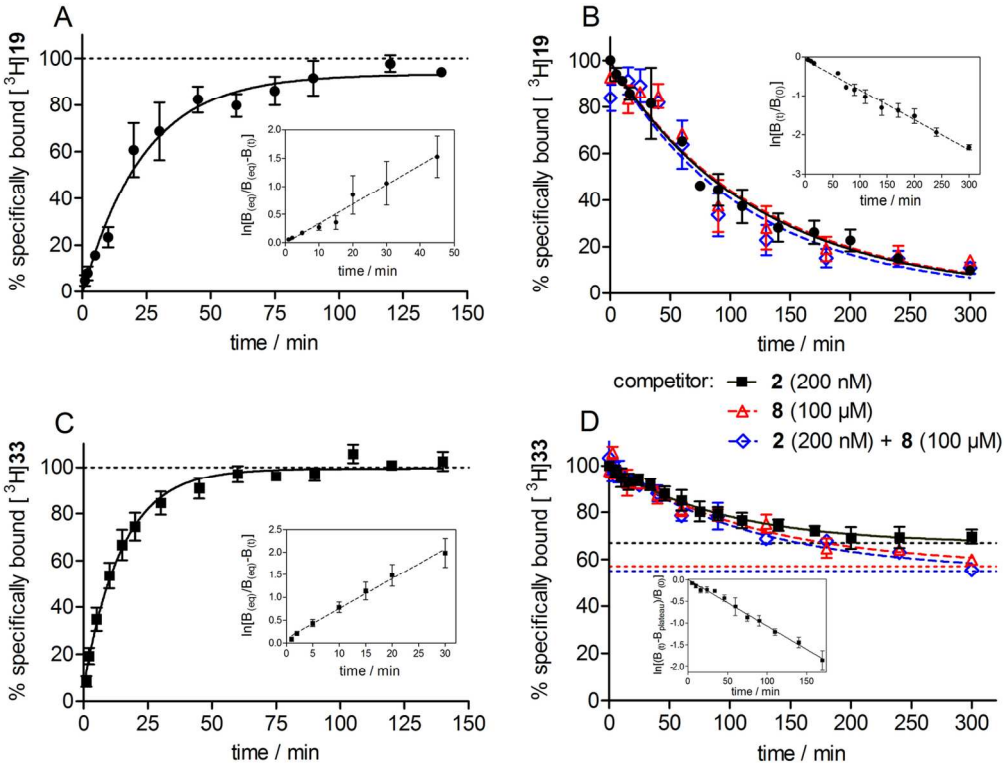

Figure 6

134x102mm (300 x 300 DPI)

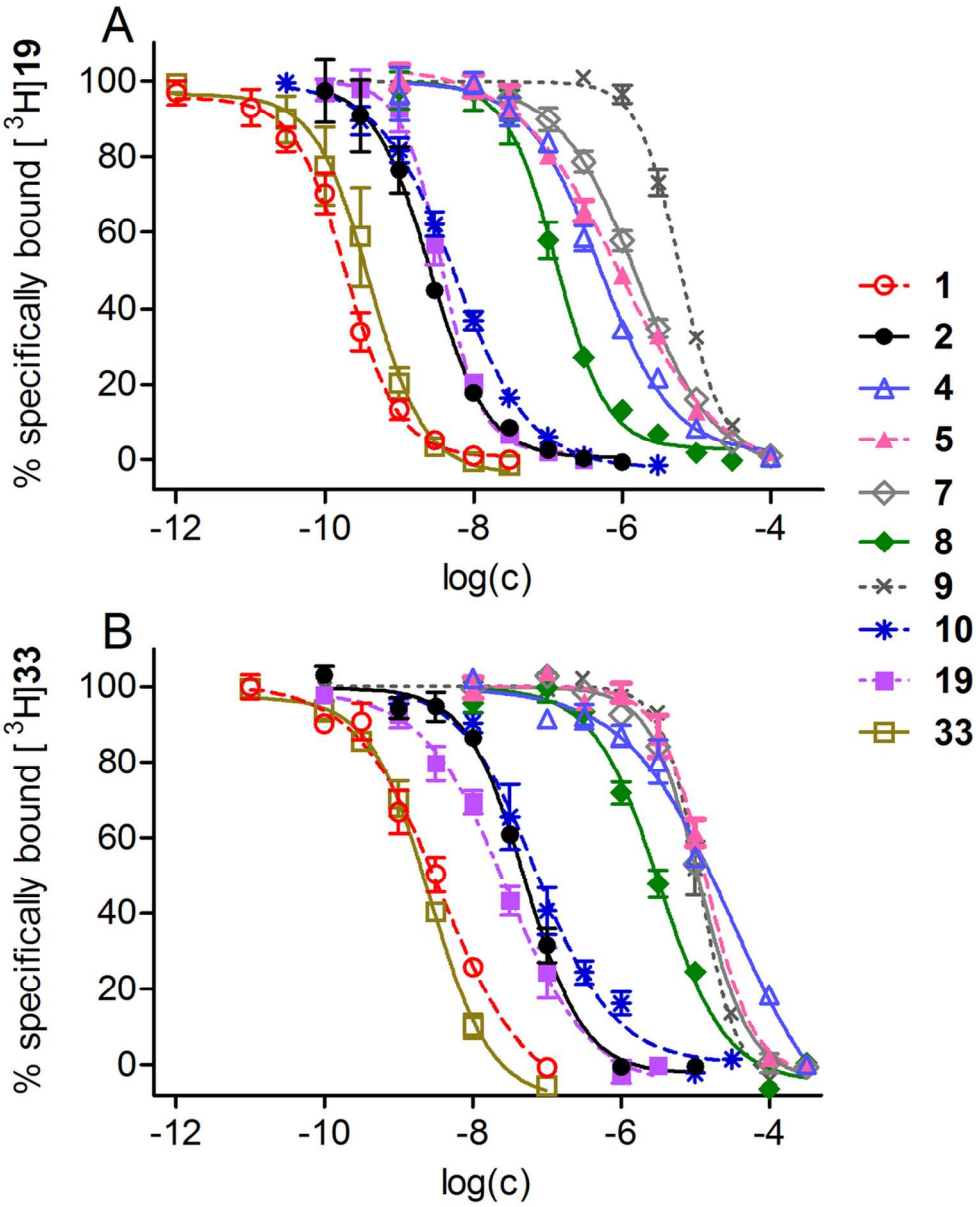

Figure 7

103x126mm (300 x 300 DPI)

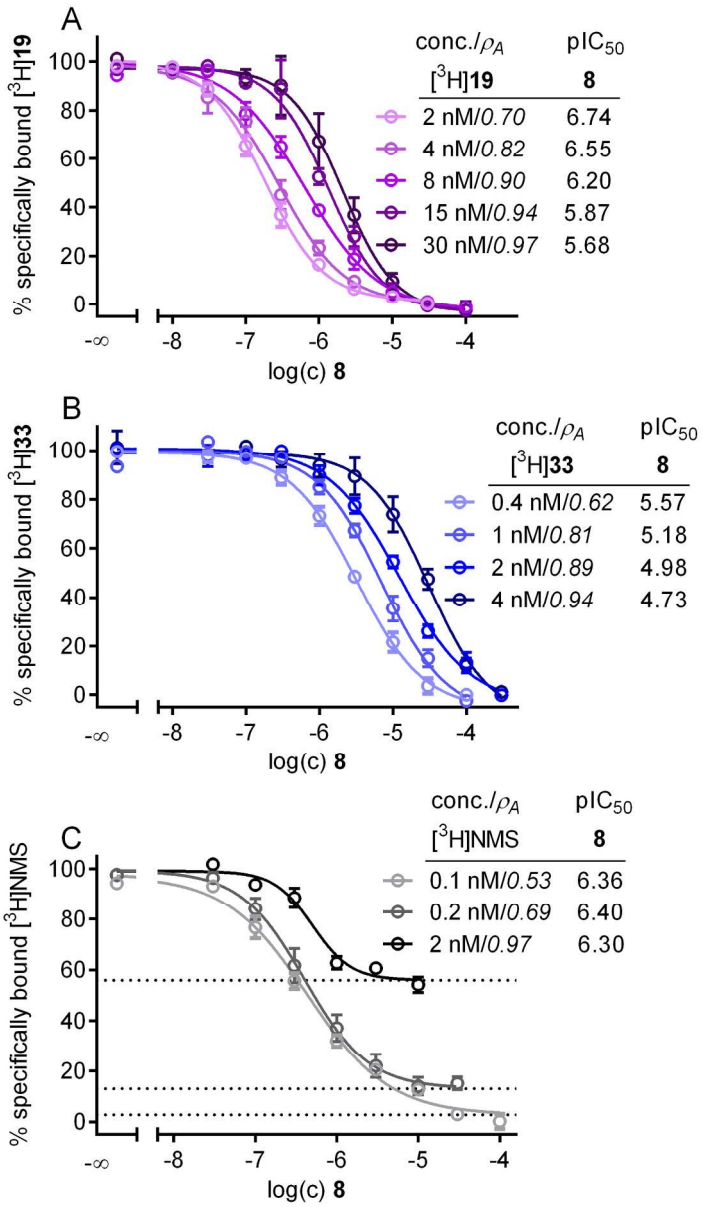

Figure 8

142x243mm (300 x 300 DPI)

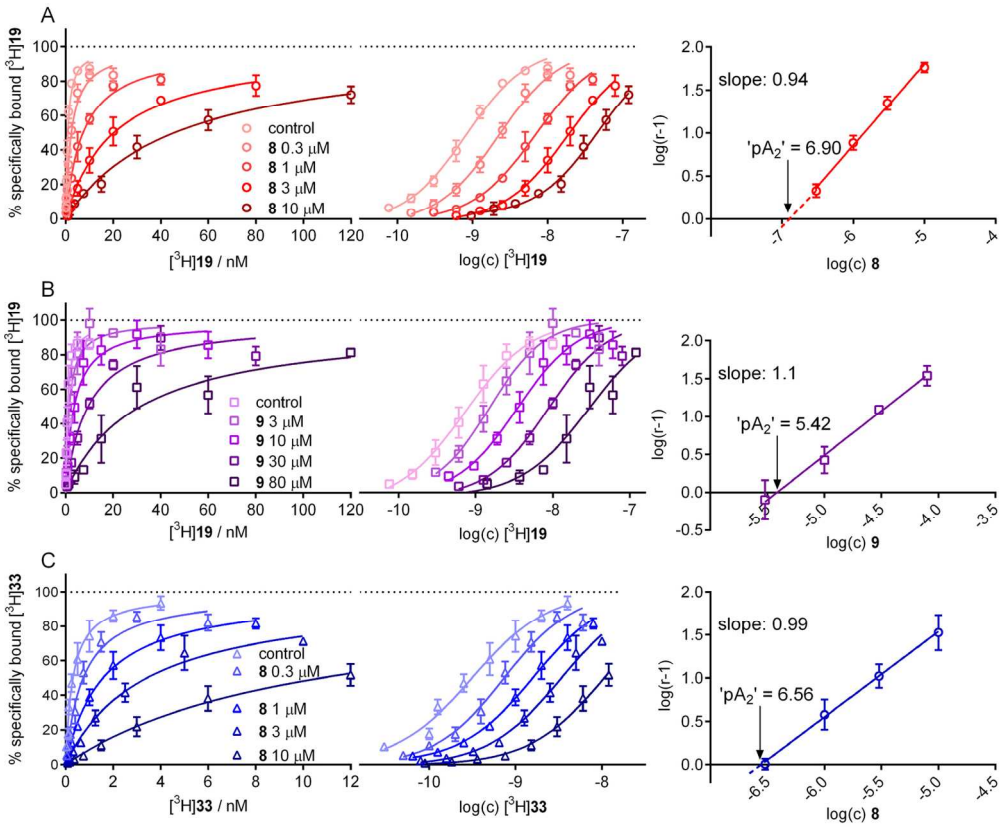

Figure 9

144x118mm (300 x 300 DPI)